NTNU

Norwegian University of
Science and Technology

Examining the geometry of Tyholt Tower using UAV, laser scanning and total station measurements

Jakub Michal Szablowski

Civil and Environmental Engineering
Submission date: June 2016
Supervisor: Terje Skogseth, BAT
Co-supervisor: Rafal Szymanowski, Reinertsen AS

Norwegian University of Science and Technology
Department of Civil and Transport Engineering

NORWEGIAN UNIVERSITY OF SCIENCE AND TECHNOLOGY
DEPARTMENT OF CIVIL AND TRANSPORT ENGINEERING

Report Title:	Date: 14.06.2016			
Examining the geometry of Tyholt Tower by using UAV, laser scanner and total station measurements	Number of pages (incl. appendices): 103			
	Master Thesis	X	Project Work	

Name:
Jakub Michał Szablowski

Professor in charge/supervisor:
Terje Skogseth

Other external professional contacts/supervisors:
Rafał Szymanowski

Abstract:

Nowadays, unmanned aerial vehicles are getting more and more popular, they are not used only in military industry, but can be found in many civilian situations. Land surveying drones has been mostly found in monitoring hazardous areas and general mapping where the application of traditional manned aerial photogrammetry is unprofitable due to the range of the project. For this thesis, author tried to check UAV possibilities in a cataloguing of construction. A high construction called Tyholt tower was chosen to be the object of interest. This tower is the landmark in Trondheim, Norway. The task was divided into two parts: the cylinder and the main gallery of the tower.

Examination of the cylinder showed that the land surveying methods: double-edged and laser scanning give very similar results of the inclination of the tower. However, point cloud obtained from unmanned aerial photogrammetry does not meet any similar results. The comparison of both: laser scanner and UAV's point cloud to the theoretical model presented that the second dataset is characterized by lower accuracy and larger noises around the object.

Studying the main gallery showed better density and comparable quality of point cloud obtained from the drone rather than laser scanner. The performance of UAV in the upper area of the tower might have been caused by numerous tie points measured with total station letting the gallery keep its proper shape.

The thesis proves that application of unmanned aerial vehicles and photogrammetry may be very helpful for examination of high construction, as well as help in 3D modeling.

Keywords:

1. Unmanned Aerail Photogrammetry
2. Terrestrail Laser Scanning
3. 3D Point Cloud
4. Industrial Surveying

_____

NTNU
Norwegian University of Science and Technology
Faculty of Engineering Science and Technology
Department of Civil and Transport Engineering

Date
19.01.2016

MASTER DEGREE THESIS

Course TBA4925 Geomatics, master thesis

Spring 2016

for

Student: Jakub Michal Szablowski

Examining the geometry of Tyholt Tower by using UAV, laser scanner and total station measurements

BACKGROUND

The ca. 120 m high Tyholt tower is a landmark in Trondheim, Norway. It is well suitable for testing different methods and equipment that can be used to determine the geometry of a high object.

TASK

The main goal of this thesis is to look into and compare the accuracy of the different data collection methods and different processing methods. The candidate is going to investigate the use of modern methods for checking the geometry of high and slim construction, the Tyholt Tower, by using unmanned aerial vehicle (UAV), laser scanner and total station. Aspects to be examined are inclinations, cloud-to-cloud comparison, quality and accuracy of obtained 3D point clouds, see the task description below.

Theoretical part

The candidate shall describe and discuss: The possibilities of how to check the condition and geometry of high and slim buildings, the surveying work and the surveying methods, the used software, and the accuracies of an UAV 3D model and a laser scanning point cloud.

Data capture

The following instruments will be used for the data capture:

Total station (Leica Viva TS15), GNSS receiver (Leica Viva GNSS GS12 receiver), UAV (DJI Phantom3 Professional), Laser scanner (Leica ScanStation C10).

Products and calculations

The analysis of the tower is divided into two parts: The cylinder and the main gallery.

Software that can be used to obtain the products and for the calculations: Pix4d mapper, Cloud Compare, Gemini Oppmåling, Leica Cyclone, Adobe Photoshop Lightroom. The software will be used for:

- Creating georeferenced 3D models of the tower from data obtained with UAV and laser scanning
- Evaluating and comparing the 3D georeferenced models obtained with the UAV and the laser scanning concerning accuracy and amount of work
- Monitoring the time and progress of conducted field and lab works

Conclusions

Evaluation of the fieldwork and post-processing. Suggestions of improvements.

Startup and submission deadlines

Startup: January 19th 2016. Submission date: Digitally in DAIM at the latest June 14th 2016.

Supervisors

Supervisor at NTNU: Terje Skogseth. Co-supervisor: Rafal Szymanowski, Reinertsen AS, Trondheim

Department of Civil and Transport Engineering, NTNU. Date 19.01.2016, (revised June 2016).

Terje Skogseth
(Signature)

Acknowledgments

I would like to express my sincere gratitude to my main supervisor Terje Skogseth for providing me the opportunity to do this thesis. I would like to thank him for all the time, support, and valuable guidance.

I am also very grateful to my co-supervisor Rafał Szymanowski for the assistance and help to do this project and all helpful guidelines.

I would also like to acknowledge with great appreciation the help from Przemysław Kuras.

I am grateful to all who contributed to this thesis.

Abstract

Nowadays, unmanned aerial vehicles are getting more and more popular, they are not used only in military industry, but can be found in many civilian situations. Land surveying drones has been mostly found in monitoring hazardous areas and general mapping where the application of traditional manned aerial photogrammetry is unprofitable due to the range of the project. For this thesis, author tried to check UAV possibilities in a cataloguing of construction. A high construction called Tyholt tower was chosen to be the object of interest. This tower is the landmark in Trondheim, Norway. The task was divided into two parts: the cylinder and the main gallery of the tower.

Examination of the cylinder showed that the land surveying methods: double-edged and laser scanning give very similar results of the inclination of the tower. However, point cloud obtained from unmanned aerial photogrammetry does not meet any similar results. The comparison of both: laser scanner and UAV's point cloud to the theoretical model presented that the second dataset is characterized by lower accuracy and larger noises around the object.

Studying the main gallery showed better density and comparable quality of point cloud obtained from the drone rather than laser scanner. The performance of UAV in the upper area of the tower might have been caused by numerous tie points measured with total station letting the gallery keep its proper shape.

The thesis proves that application of unmanned aerial vehicles and photogrammetry may be very helpful for examination of high construction, as well as help in 3D modeling.

Table of Contents

List of Appendices

List of Figures

List of Tables

1. Introduction

The aerial photogrammetry with usage of Unmanned Aircraft Vehicles is getting more and more common, as the market booms in the civilian drones' industry. The fact is that the applications of the UAV are countless and they are tested in every field of life to help, ease or allow to do things too expensive or too difficult to achieve before.

From simple applications like taking pictures and shooting movies from important events, through using UAVs as a mean of transport for small objects, ending up at taking pictures for photogrammetry applications which are characterized by high accuracy and precision for deliverables. The engineering applications are also vast, the most known are aerial unmanned photogrammetry for monitoring hazardous areas, making orthophotomaps, general mapping for smaller areas where usage of manned aerial photogrammetry is economically inefficient.

In the common trend of challenging possibilities of UAVs, the author decided to test available drone (DJI Phantom 3 Professional) in terms of engineering inventory of high construction. Author formulated the hypothesis:

Can drone be compared to the land surveying methods in terms of accuracy?

For this comparison author selected two land surveying methods double-edged method and laser scanning method. The justification of selection of these methods is that the first one was used basically since the beginning of surveying high construction to check their inclination. The second one is way more advanced, High Definition Surveying provides huge datasets of spatial points taken at the site, which helps to investigate the inclination of the object as well as an overall view of the construction. The mentioned construction is the landmark of Trondheim city and also a TV- and radio- transmitter tower.

1.1. Object of interest

Tyholt Tower is a well-known landmark of Trondheim city. It was built in 1985 and designed by an architect called Nils Christian Ottesen. It is about 120- meters high, including around 40- meter mast. It is telecommunication- and radio tower, which works as a platform for a television and FM-transmitters. The tower is erected at 112.5 meters above sea level. There is a restaurant at the top of the tower (70 meters above the ground), which attracts tourists with its outstanding panoramic views. Moreover the upper floor of the restaurant does a 360 degrees rotation per hour. The name Tyholt is related to the district of the city, where the object lies. Buildings which surround the tower are short, as they do not have more than 4 stories, and development of the area is rather loose, which make access to tower easy and safe.

Figure 1 - View of Tyholt Tower [https://tchile.wordpress.com]

We can divide the tower into 4 parts, a most bottom is the building where is the entrance to elevators leading to the top of the tower, the cylinder with landings and supportive elements for transmitters, the main gallery inside which is the restaurant and finally the steel antenna mast.

Only two of them are going to be described in detail, which are: the cylinder, without elements attached to it and main gallery which shape is an upside-down 12-sided truncated pyramid (frustum), made of steel and glass. The entrance part and the mast, will not be covered up in this thesis because of theirs simplicity and difficulty in shape, accordingly. As for the mast it is very hard to predefine the cross-sections, plus long distances and small surfaces are a big problem for measuring methods.

1.2. Methods

Towers are classified as slim buildings category. Those buildings are defined by their maximum width to height ratio. In this category, we may find my engineering and industrial construction such as cooling towers, industrial chimneys, FM- and TV-masts, headframes (using in underground mining), lighthouses, observation towers and high pillars (of bridges).

Figure 2 - Examples of high constructions [Multiple sources, google graphics.]

There are many factors, which cause slim buildings change their location or geometry. Beginning with chemical factors, which are changing the structure of construction material. Phenomena such as stress relaxation and rheology, are responsible for reducing inner stress over time and taking into account the impact load on the behavior of structural materials in dealing with the duration of these loads. The last chemical phenomenon is related to rain, it affects material like steel or concrete and leads to decreasing the quality of construction material.

Mechanical factors are associated with soil properties, wind and mining exploitation. It is natural that newly erected buildings will start settling, and the expected maximal settlement is tens of centimeters and it is equal to the whole area of foundations. The bigger settlement is the higher risk of replacing the facilities like electricity and water. The most dangerous for high constructions

are inclinations of the plumb line of the construction, due to an uneven settlement of foundations, no matter if it is a big or low settlement.

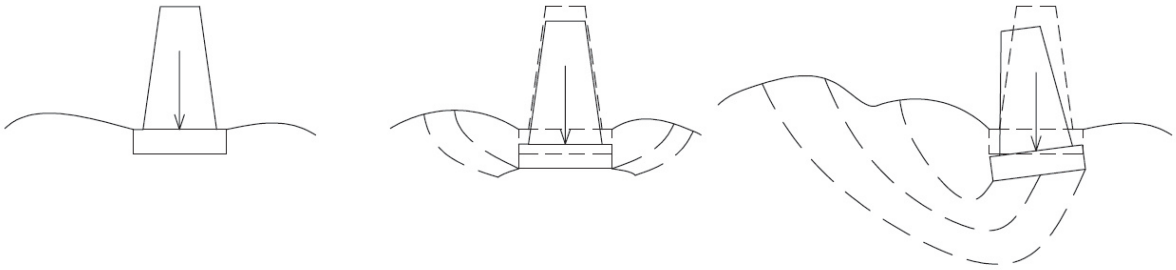

Figure 3 - Settlement of a construction.

The wind is also harmful for slim construction. Large lateral surfaces may encounter high wind pressure. Besides that, the biggest fear is vibrations which can be human-induced by conducted technologic processes. Vibrations occur also due to technical devices making their own as well as random phenomena, not caused by human, for example, earthquakes. As a well-known textbook example of the destructive power of forced resonance is Tacoma Narrow bridge collapse. In autumn 1940 in the U.S. state of Washington, over 1800-meter length bridge had collapsed due to the wind, which had a speed of approximately 60 km per hour. Unfortunately, the wind provided an external periodic frequency that matched to the natural frequency of the bridge.

When we deal with the underground mining exploitation area, we should be careful with projecting high construction even more. The basin, made because of the exploitation, has usually vast range, and its depth depends on the thickness and depth of exploitation. There are some methods to prevent or at least reduce deformations and bad influences of underground mining.

The last, but not least factor changing the geometry of high and slim constructions is sun. Heat and daily temperature differences cause stretching and extending of the construction material. Each material has its own thermal expansion value, for example, steel and concrete have rather similar linear thermal expansions, for steel it is 10-17 m ($10^{-6}K^{-1}$), and for concrete 14.5 m ($10^{-6}K^{-1}$).

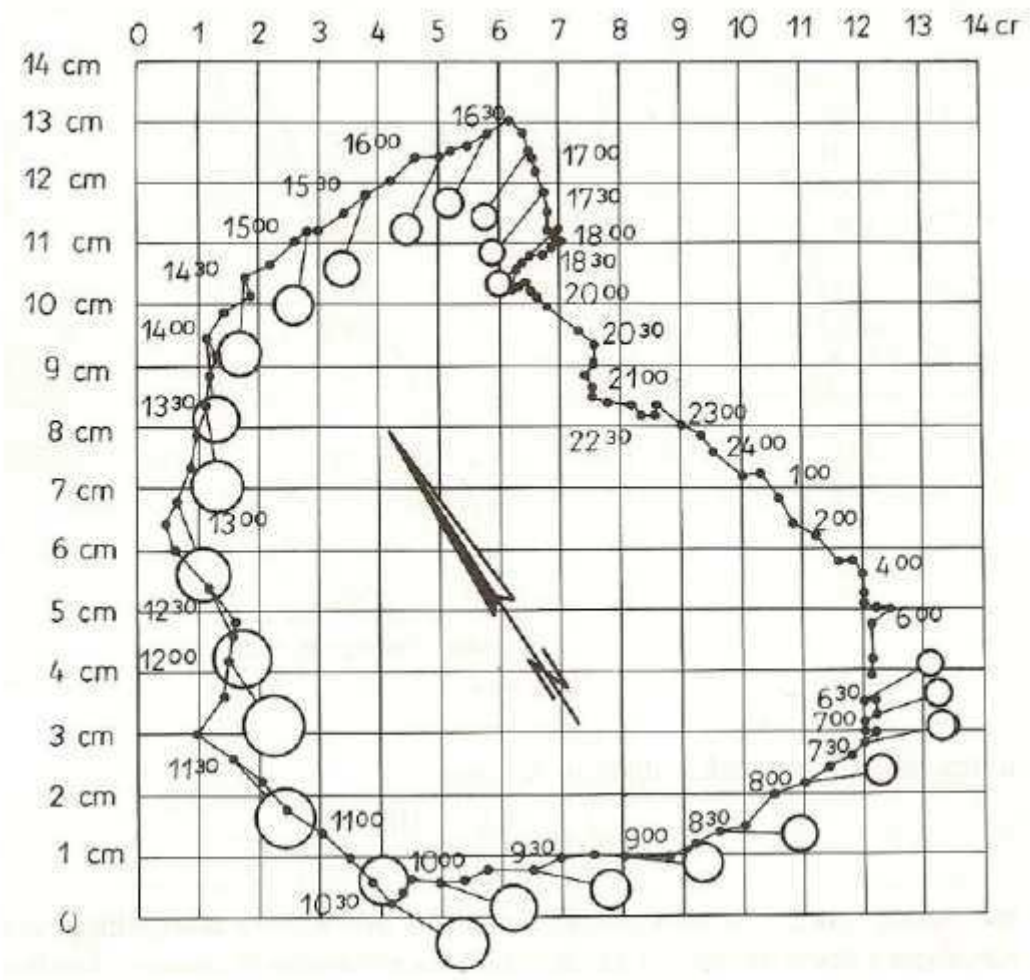

Figure 4 - Daily movement of the 275m industrial chimney [19].

1.2.1. Precise leveling

Inventory of slim constructions is conducted if settlement of foundations and inclination are checked. The settlement can measured only by leveling. Benchmarks situated on the cover of towers or industrial chimneys have to be measured in order to calculate the rotations (in 3 planes). Some of the industrial chimneys reach even 300 meters (right now it is less likely to build chimneys that tall because the flue-gas desulfurization methods have improved), so this is extremely important to conduct precise leveling procedure. Proper technical leveling procedure gives only 1-millimeter accuracy heights, whereas precise levelling gives 0.1-millimeter accuracy.

A table shows the difference in rotations along axes for the same industrial chimney using 1 mm and 0.1 mm-accuracy in the height of measured benchmarks.

Table 1 - Local coordinates of exemplary benchmarks on chimney's foundation with differences in heights upon the time, and calculated settlement and rotations.

X [m]	Y [m]	dZ [mm]
3.538	3.895	-1.7
-0.344	5.251	-0.4
-3.236	4.149	-0.9
-5.260	-0.119	-1.9
-3.332	-4.073	-1.8
0.833	-5.196	-1.6
5.044	-1.500	-0.6

X [m]	Y [m]	dZ [mm]
3.538	3.895	-2
-0.344	5.251	0
-3.236	4.149	-1
-5.260	-0.119	-2
-3.332	-4.073	-2
0.833	-5.196	-2
5.044	-1.500	-1

-1.27	$=dZ_0$ [mm]
0.07	$=\omega_x$ [mm/m]
-0.06	$=\omega_y$ [mm/m]

-1.46	$=dZ_0$ [mm]
0.11	$=\omega_x$ [mm/m]
-0.03	$=\omega_y$ [mm/m]

The points described above are benchmarks at the foundation of a high construction. X and Y are in a local coordinate system, with an origin in the center of the object. Values in the last column (dZ) are the differences between height coordinate separated in some period of time. It is easy to notice that these values are small, so we have to put more effort to obtain trustworthy results. Using this as an example, the author would like to show the difference between 0.1mm and 1.0mm accuracy, rotations of the x-axis (ω_x) and y-axis (ω_y) do not match. Having a 100-meter tower (which is very probable), the maximum inclination would be accordingly 9mm and 12mm. Taking up this example for the highest industrial chimney in the world – GRES-2 Power Station in Ekibastuz, Kazakhstan – which has 419.7 meters, the difference is over four times larger.

1.2.2. Protractor methods

There are many methods to determine the inclination of high and slim objects. Some of them can be conducted with the use of protractor equipment (for example Zeiss Theo 010, T2 Wild) and Total Stations (Leica TC407, Leica Viva TS15), these methods are direct projection, indentations, double-edged angles and method using mirrorless measurements- polar method. They allow defining the trajectory of object's axis at selected levels. This thesis explains briefly every method, but only one was used during field measurements – double-edged angle method.

1.2.2.1. Direct projection

This method is using meter stick – big ruler, situated under the exanimating object, perpendicularly to a station, and in the horizontal position. It directly provides values of inclinations at selected levels, with respect to base level at the most bottom. Aiming at a first

defined level at the edge of an object, and then only moving scope of an instrument, we note down the value from the ruler. Repeat this for every selected section in both faces of the instrument, to exclude instrument's errors, and for both edges of the tower. There should be at least two stations and they ought to make 90 degrees angle with the object. If we established more than two stations, they should make a regular polygon, with the object as the center. Direct projection method allows to get values of inclination at the site, the only thing to present plots/graphs is the calculation of the heights of selected levels. Direct projection is used only for objects with a considerably small span of cross sections.

1.2.2.2. Polar method

The method is based on mirrorless measurements. Having established station with local (or global) network, we measure distances and both angels to points at selected levels. Points cannot be very close to the edges of construction, because of errors in measured distance. [12] This is the way we obtain a representative cloud point, which is a base for calculations of the centers of the construction.

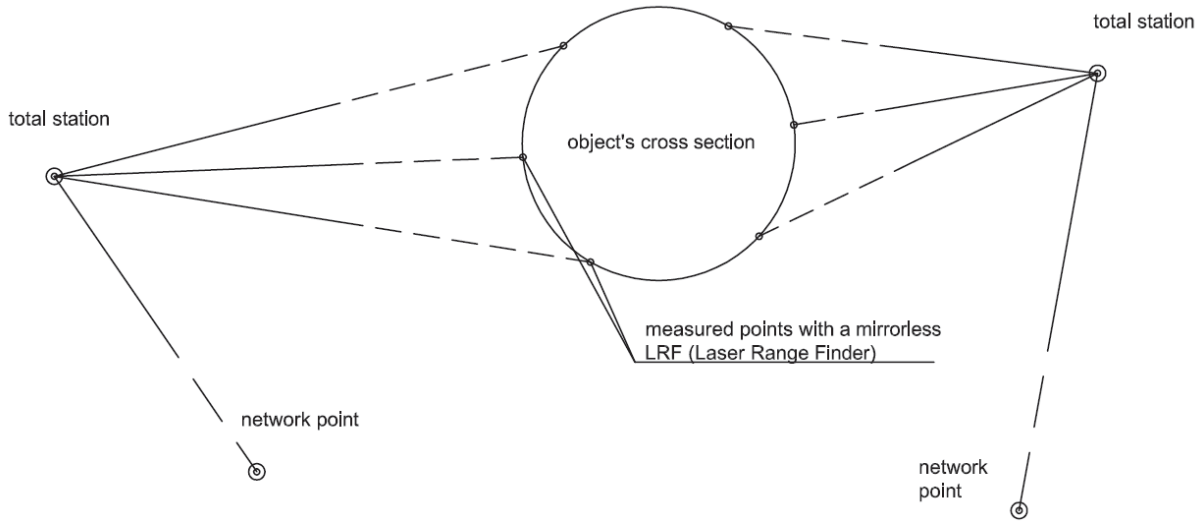

Figure 5 - Visualization scheme of the polar method.

The more advanced approach of a polar method is HDS (High Definition Surveying), which is going to be covered in next chapter.

1.2.2.3. Intersection and double –edged method

These two methods are very similar, in terms of measured points in both we aim at the edges of the examined construction, and we read only angles. However, requirements and calculations process differ from each other. Intersections' approach works on spatial coordinates

of the geometrical center for each cross-section level and with simple coordinates' subtraction. We obtain deflection between selected levels. Moreover, when this method is conducted with more than two stations, we have to increase theirs coordinate's order of accuracy to 5mm [8].

$$w_X^j = X^j - X^0$$

$$w_Y^j = Y^j - Y^0$$

where:

w_X^j, w_Y^j – component inclination in X or Y direction,

X^j, Y^j, X^0, Y^0 – coordinates of cross sections' centers at j-th and reference level.

On the other hand, the double-edged method needs more complicated calculation process, and works with small angles- this is going to be presented in detail in chapter 4.1. Thanks to this, network coordinates can be determined even within +/- 1-meter accuracy.

1.2.3. Other methods

There are also methods using non-surveying equipment to conduct the inventory of the slim constructions. Thermography, MEMS (Micro-Electro-Mechanical Systems), laser and photosensitive panel. Thermography has the largest influence in industrial chimneys, where the objects are exposed to high temperatures inside the cores of a chimney, and also from the outside- caused by the surrounding facilities.

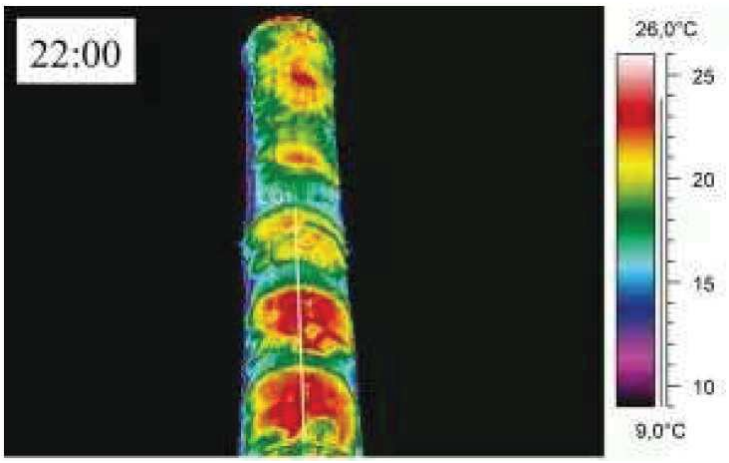

Figure 6 - Thermography, coat of an industrial chimney [18].

This method is helpful to identify the isolation inside the chimney's core. It is expected the heat is equal to the whole object if the isolation works properly. Otherwise, coat's parts with higher temperature are more likely to be damaged, which leads to degradation of the construction's quality.

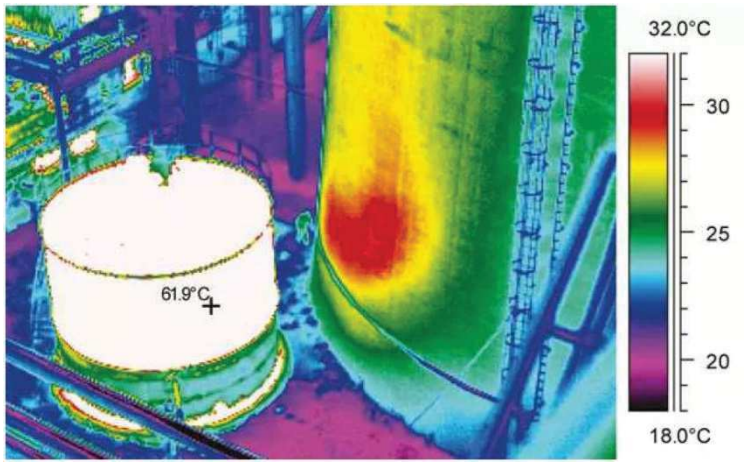

Figure 7 - Thermography, the heated part of coat, caused by surrounding object [18].

Micro-Electro-Mechanical Systems have a vast range of applications. Using them in high objects surveillance, MEMS accelerator detects the inclinations through the effect of gravitation in three planes. We obtain similar results if we put GPS antenna at the top on object, or use a laser at the top pointing down and a photosensitive plate mounted on the foundation of the object, then we obtain differences in coordinates- for laser and photosensitive plate, there is a need to calibrate sensor and transformation from pixel system to linear system (for example millimeters). These methods provide only generalized inclinations of the object, in other words we have no clue what is happening between the foundation and the top of construction.

1.2.4. HDS and UAS as more advanced techniques

Using protractor methods we have a small dataset as a result, and upon that we need to spend considerably long time at the site to obtain them. Nowadays, surveyors have a possibility to spend the same amount or shorter time at site applying more advanced techniques such as High Definition Surveying (HDS) and Unmanned Aerial System (UAS), those give huge dataset. Thus, storing and processing them could be an individual subject of the thesis.

1.2.4.1. High Definition Surveying

This technique requires a modern equipment such as laser scanning station. Nowadays, surveyors have a vast market of these instruments. Many companies try to improve their technologies to contest with competitors in terms of speed, accuracy, and price of an instrument. The most recognizable terrestrial laser scanning station brands are Leica Geosystems, Trimble, Faro and Riegl. Each of them has their own series of instruments which differs in range and purpose. As an example, Faro has a Laser Scanner Focus^{3D} X-Series, which contains three models

of laser scanning station – X30, X130, and X330. The number indicates the maximal possible range of laser scanner, and so the shortest range scanner could be used for small architectural facades, complex structures, production and supply facilities and accident/crime scenes. The mid-range laser scanning station on top of the short-range one may conduct measurements of large-volume components. Whereas, the extra long-range can cover all mentioned tasks with a higher precision and accuracy. The manufacturer says that all the models have accuracy up to +/- 2 mm, but according to [12], it is hard to obtain such a good results, when the surfaces of objects differs from each other [13]. The color is important as well as whether surface is wet or dry.

Buying one of those scanners, the surveyor has to know kind of challenges he is going to meet because the price for the short-range and extra long-range scanning station is almost twofold higher.

Laser scanning station is helpful, or even irreplaceable, for challenges, like:

- planning and early design stages of erecting constructions,
- topographic surveys,
- detailed elevation surveys,
- accident investigations,
- archaeological sites,
- rights of light report,
- 3D printing of site model,
- Building Information Modelling (BIM),
- monitoring land deformations,
- preserving historic buildings,
- volume surveys,
- post-construction scans for the cataloguing process.

If we consider traditional survey and 3D laser scanner technique on an example of surveying a complex architecture [16], the author of this article conducted many building surveys, and describes his observations using both methods, listing strengths and weaknesses of them. Of course, one's pros are the other's cons.

The classical approach for the task requires two-stage measurement. The first step is the topographic survey, while we measure the position of some essential point, such as vertexes of measured property, doors, windows or nodes of rooms. Later these points are used for direct

surveys- step two, while direct surveying worker uses portable laser device. There is no need to pay attention to how measurements will be joined together because for global positioning we use pervious step- topographic survey.

3D laser scanner surveying provides a huge dataset of points, as it is creating so-called 'cloud point'. The surveyor has an impact on the extent of the dataset by determination of scanning resolution, which depends on the size of space, and mostly the size of acquired details. The most important thing is overlap between neighboring scans, during post-processing overlapping part will be used to join scans into the whole scene, these complex calculations are called 'cloud-to-cloud registration'. There is a possibility to increase the accuracy to the whole scene through an application of HDS targets - these are the spots measured with a total station before scanning operation. Overall time spent at the site will extend, but accuracy should increase, and we may avoid the cloud-to-cloud registration.

The acquisition of point clouds grants few advantages over classical approach, such as:

- fast acquisition of data, saving time spent at site,
- no need to be concerned about the lack of obtained data, the scanner is measuring 360 degrees horizontally and about 300 degrees vertically,
- very convenient for measuring inaccessible areas,
- possibility to present space as the 3D model, not only the traditional 2D cross-sections.

About the disadvantages we should highlight:

- high initial cost of investment,
- software able to handle point clouds,
- expensive hardware for post processing.

Despite weaknesses of 3D scanning method, it is getting more and more popular. The range of applications is vast and surveyors are more eager to use it. Next method booms at the surveying market, but not only that. Unmanned Aerial Vehicles (UAVs) are present in our lives as toys, racing vehicles or sophisticated platforms making pictures.

1.2.4.2. Unmanned Aerial System

Introducing this new technique, in author's opinion, we should get familiar with names and acronyms. Thus, UAS stands for Unmanned Aerial System, as the title of this chapter, but there are more names for this. For example, UAV stands for Unmanned Aerial Vehicle, the main difference between those two is that UAS relates to the vehicle, communication segment, and the

adjuvant software – called ‘ground control station’. UAV and drone are most common terms, whereas the second one has a rather negative reputation, it is due to this term was used first at military field. On a side note, many military inventions were translated to civilian world improving our lifestyle, for instance: GPS, Internet, microwave oven, the digital camera, etc.

Nowadays, drones are becoming more and more common device. People use them as a hobby or extraordinary digital camera. There are plans to revolutionize transport, using drones as an autonomous carrier for courier companies. As surveyors, UAVs are used mostly for mapping, quoting Ismael Colomina and Pere Molina “Let them fly and they will create a new remote sensing market in your country” [4]. Indeed, possible applications in mapping are huge and it is a real threat for aerial photogrammetry using airplanes, due to high initial and post-processing costs.

In the opinion of two presidents of polish photogrammetry-related MGGP Aero Company [11] - having great experience in the field - who speak about acquiring material used for ortophotomaps, the classical manned aerial photogrammetry is in good shape. They justify their attitude, explaining flaws of some UAS applications. For instance, they brought up a project for a sewage plant in Poland to create ortophotomap using UAV, it needed to take 900 photos. Nonetheless, to meet the requirement of accuracy for each Ground Control Point should be 20-30 photos. The presidents estimated that for the classical aerial they would need 4 GCPs. The large difference transfers to time spent for post-processing. Although, they admit that UAV measurements are sufficient and economically better for small and point projects. One of the undeniable advantages of manned aerial photogrammetry is the possibility to mount various, heavy sensors in the airplane, such as hyperspectral cameras, thermovision cameras, and laser scanners. Moreover, big and heavy aircraft are more resistant to weather conditions such as wind, therefore, the angles of three axes of rotation (yaw, pitch, and roll) help to obtain more accurate results, especially important for large areas.

Table below shows applications and features of manned aerial photogrammetry, terrestrial close range photogrammetry and unmanned aerial photogrammetry.

Table 2 - Features and applications of terrestrial close range photogrammetry, manned and unmanned aerial photogrammetry [9].

	Manned aerial photogrammetry	Terrestrial close range photogrammetry	Unmanned aerial photogrammetry
Coverage area	> 100 km^{2*}	1-3000 m^2	100 m^2 - 100 km^2

GSD	0,05-0,5 m	0,001-0,01 m	0,01-0,30 m
Distance from object	100 m-10 km	1-500 m	10 - 1000 m**
Rest of application and features	coverage of extensive areas (glaciology, forest mapping, cities 3D modeling)	coverage of small areas, documentation of antique buildings, buildings 3D modeling	coverage of small areas (large-scale), documentation of antique buildings, buildings 3D modeling
		architecture, engineering photogrammetry	application at inaccessible or dangerous sites
	aerial perspective	terrestrial perspective	aerial perspective
			monitoring in real time

*minimal coverage area- economical aspects

** maximal high value, legal restriction in different countries

In author's opinion, it is important to compare all possible techniques in land surveying, defining a relation between accuracy and object/area size. Figure 8 presents mentioned comparison.

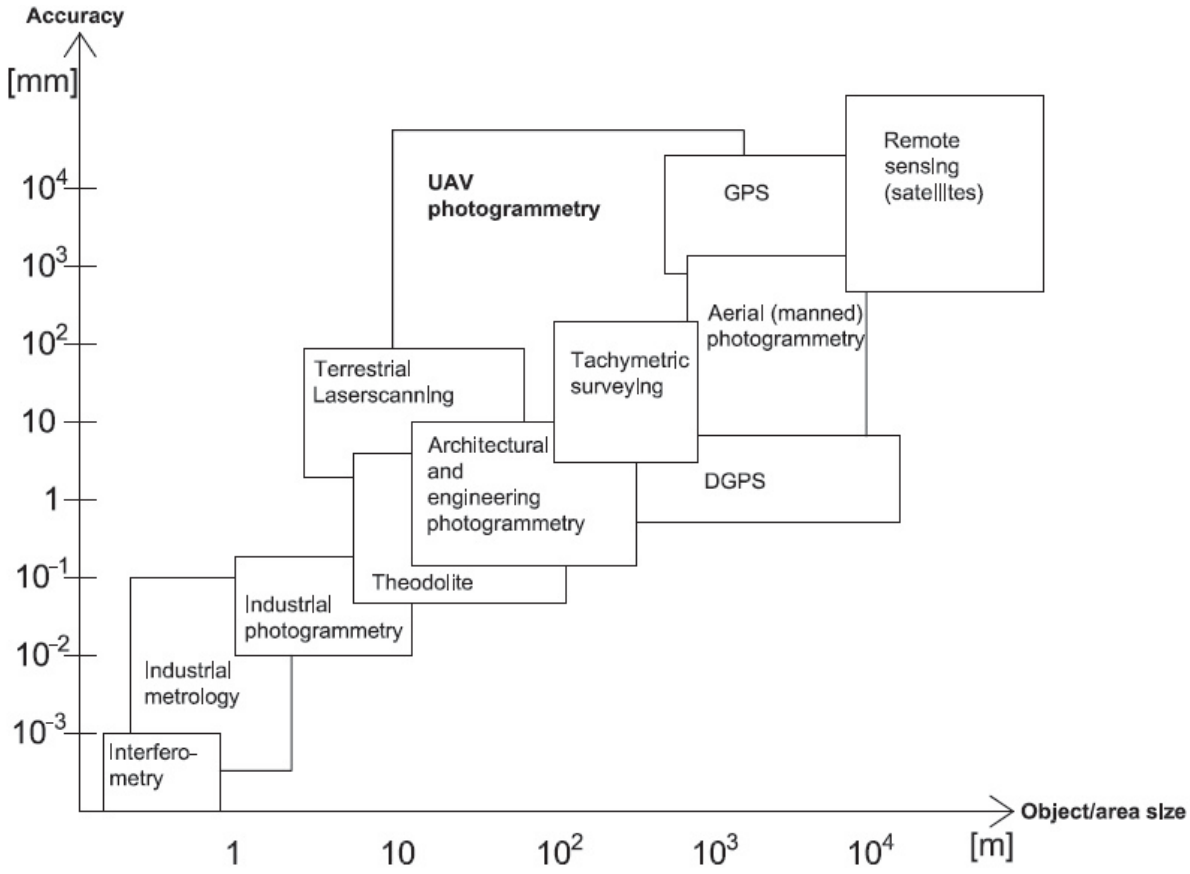

Figure 8 - Accuracy of methods used in land surveying [5].

Let us notice, that UAV photogrammetry touches many known techniques like GPS, terrestrial laser scanning, tachymetric surveying and classic aerial photogrammetry. Each technique has its own purposes and applications, and unmanned aerial systems are an alternative to expanding surveyor's point of view, and in some situations let him choose between techniques, depending on requirements of the project. It is also possible to choose a less accurate technique, and probably reduce the costs of the task.

Thanks to the introduction of unmanned aerial photogrammetry, it is possible to conduct a visualization method for small areas. It also allows connecting aerial photogrammetry and terrestrial one, giving the opportunity to increase the accuracy at particular projects.

2. *Software*

The software is as important as the technique of measurement. Every user wants to receive the same results each time, and as fast as possible. In addition, for the users' convenience, the interface of a program should be intuitive, and followed up with a 'help' file and brief descriptions of functions.

Each program is designed to the same task differs from another, due to implemented algorithms and - most likely - the code. Working on this thesis, author used one program for each part of data post-processing, the choice was conditioned by the availability and - in one case - by the surveying instrument–software compatibility.

2.1. Gemini Oppmåling

It is the software used for basic purposes in classical land surveying. The interface is simple and provides easy access to all available features, helping with tasks such as:

- Importing and exporting data sources,
- Conducting calculations with different methods,
- Adjusting network,
- Checking geometry of network,
- Analyzing accuracy,
- Preparing documentation,
- Plotting maps and field sheets.

Company Powel, the producer of Gemini Oppmåling, also have software dealing with 3D drawing and point clouds management. Nevertheless, the author has used another software delivered by the Company Leica Geosystems presented in next subchapter.

2.2. Leica Cyclone

As mentioned before Leica Cyclone 9.0 provides great compatibility with used in field work laser scanning station Leica ScanStation C10. Whole Leica High Definition Surveying software is divided into many modules, which execute particular task managing dataset.

Leica Cyclone Register Module is probably the world's most known software for georeferencing and registering laser scan datasets to defined coordinate system. Registration is the process of combining laser scans into one scene. There are two ways to achieve this, one of them is using HDS targets, where few targets are mutual for neighboring scan stations, and the second one is joining manually overlapping scan stations in pointed sections. This method does not set the georeferenced. We need to add some measured points like HDS targets to achieve geographically referenced results.

Model Module of Leica Cyclone package allows users to directly process point clouds into geometric objects and then to export them into CAD program. The greatest feature is that multiple users can work on the same datasets simultaneously reducing time-consuming tasks. A very helpful feature is also pipe-finder, which automatically finds cylinder-shaped figures. The sub-program of Model Module is Survey Module which helps surveyors to quickly attain specific details and spatial coordinates from datasets, and create cross-sections or profiles, creating TIN and Mesh, and calculating volumes and areas.

Leica Geosystems also provides more modules for Leica Cyclone such as:

- Basic – in the field, is used to manage scan parameters, field Quality Accuracy, digital imagining and target scan acquisition; in the office, is used to view and navigate point clouds and 3D models.
- Importer – provides import capability for third-party laser scanners for instance Riegl and Faro, in neutral formats (ASCII, PTS, PTX, and PTG)
- Server – allows for simultaneous access to datasets, creating good environment for extensive projects
- Publisher and TruView – create point clouds and 3D models files and share on the Internet, which allows everybody to access to them anytime.

2.3. Pix4D mapper

Pix4D mapper v.2.0.104 is a product of Swiss company, created for classic aerial, close-range (terrestrial) and UAS photogrammetry. The program allows creating 3D point clouds, triangle meshes, and ortomosaics from taken pictures. As a new feature, it is also possible to make output products basing on captured movies. However, picture resolution is usually higher than the movie. The resolution is essential for finding automatic tie points between 2 or more pictures, which translate into future accuracy and density of point cloud.

Pix4D offers great self-training options, starting from manuals and forum, through videos and webinars, ending at personal training tailored for specific purposes and problems. The software is touching all photogrammetry methods, which can be used in fields like:

- construction – documenting construction site from aerial view,
- agriculture – capturing the range of fields and calculating NDVI (Normalized Difference Vegetation Index),
- mining – surveying open-pit mines more safely,

- emergency responses – for estimating the extent and magnitude of natural disasters,
- cartography – making maps faster,
- real estate – presenting property as 3D model.

2.4. Cloud Compare

Cloud Compare v.2.6.2 is an open-source project started in 2004 by Daniel Girardeau-Montaut in France. The first intention of the software was performing a comparison between two 3D point clouds or point cloud and a triangular mesh. With time, the open-source software gained many new features becoming very comprehensive tool for 3D point cloud (and triangular mesh) management. At the moment, users can conduct alignment and registration of many point clouds, create geometric shapes such as planes, spheres, 2D polygons and quadric surfaces, and make a comparison between modeled surface and point dataset. When the dataset is larger than your hardware can handle with, it is possible to subsample data set using random, distance, octree method for smoother and faster processing.

3. Field work

Author and co-supervisor conducted field work in two days. The main indicator for choosing measurement days was similar atmospheric conditions, such as the amount of sunlight (insolation) and air temperature. These two factors have the biggest influence for the object's inclination, which is the basic comparison between all measurement methods. All field work preceded terrain overview, while the laser scanner and total station stations were established approximately to see the line of sight between each other.

3.1. Coordinate systems

Land surveying deals basically with coordinates, the author had to set the local network, in global coordinate system. There are two official coordinate systems in Norway, EUREF89-UTM (zones: 32, 33 and 35) which is in use onshore, the second one, ED50-UTM, is in use offshore.

Until the year 2011, in Norway was in operation NN1954 vertical datum. This datum delivered orthometric heights (above mean sea level). In year the 2011 was introduced new vertical datum – NN 2000. The reason for that was the post-glaciation, land uplift and also - in a lesser extent - sea level rise.

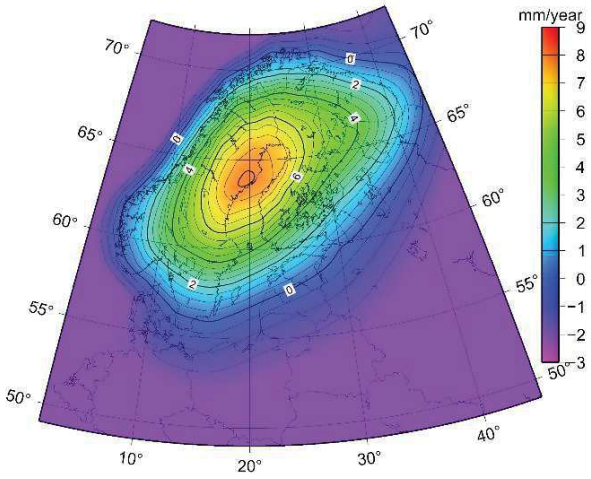

Figure 9 - Land uplift after the post-glacial period. [20]

The real heights of benchmarks have changed from 0 to 30 cm in the time course of about 50 years. Thus, the solution was to introduce new vertical datum, which should last for some future decades. The new height coordinate system refers to the geoid (it agrees with the mean sea level at reference year).

3.2. Equipment

During field work, a vast range of equipment was used. Starting from GNSS receiver Leica Viva GNSS GS12, total station Leica Viva TS15, laser scanner Leica ScanStation C10, and unmanned aerial vehicle DJI Phantom 3 Professional.

Leica Company with their instruments allows conducting all survey one-person, thanks to attached 360˚ reflector on the pole and on top of that GNSS antenna. Equipment is compatible with one another, so the offset between the center of a reflector and the antenna reference point (ARP) is included in calculations. Automatic Target Recognition is also very useful feature in the total station Leica Viva TS15, which allows it to follow 360˚ reflector and measure points: continuously, or every declared distance/time or in mode Stop&Go, in which user manually stops on the measured point and with a use of controller orders total station to start measuring.

Table 3 - Characteristics of Leica Viva GNSS receiver GS12. [http://www.leica-geosystems.com].

GNSS Technology	*Advanced Measurement Engine*	
	Leica patented SmartTrack technology	• *Jamming-resistant measurements* • *High precision pulses aperture multipath correlator* • *Excellent low elevation tracking technology* • *Very low noise GNSS carrier phase measurements with <0.5 mm precision* • *Minimum acquisition time*

	Max. simultaneous tracked satellites	*Up to 60 Satellites simultaneously on two frequencies*
	GNSS Measurements	
	Satellite signals tracking	*GPS: L1, L2, L2C, L5 (C/A, P, C Code)* *GLONASS: L1, L2 (C/A, P narrow Code); Galileo: E1, E5a, E5b, Alt-BOC;* *SBAS: WAAS, EGNOS, GAGAN, MSAS*
Measurement Performance	***Accuracy (RMS)[1]***	
	Network RTK	*Horizontal: 8 mm + 0.5 ppm* *Vertical: 15 mm + 0.5 ppm*
	Post processing (phase) Static with long observations	*Horizontal: 3 mm + 0.1 ppm* *Vertical: 3.5 mm + 0.4 ppm*
	Post processing (phase) Rapid static mode	*Horizontal: 3 mm + 0.5 ppm* *Vertical: 5 mm + 0.5 ppm*
	On-The-Fly Initialization	
	Reliability[1]	*Better than 99,99% using Leica SmartCheck technology*
	RTK baseline range	*Up to 70 km*
	Data Recording	
	Recording rate	*Up to 20 Hz*
Hardware	***User Interface***	
	Communication ports Lemo plug	*• Combined USB / Power port with 8-pin* *• Integrated Bluetooth® port* *• 5-pin clip-on contacts for Leica SmartStation setup*
	Communication Protocols	
	Real-time data formats for data transmission	*RTCM 3*
	Real-time data formats for data reception	*Leica proprietary formats (Leica, Leica 4G), CMR, CMR+,* *RTCM 2.2, RTCM 2.3, RTCM 3.0, RTCM 3.1, RTCM 3.2 MSM* *Full support of RTCM 3 Transformation Message*
	Physical	
	Weight	*1.05 kg including battery*
	Dimension (diameter x height)	*186 mm x 89 mm*
	Environmental Specifications	
	Temperature, operating	*–40° C to +65° C, compliance with ISO9022-10-08, ISO9022-11-special, MIL-STD 810G Method 502.5 II, MIL-STD 810G Method 501.5 II*
	Temperature, storage	*–40° C to +80° C, compliance withISO9022-10-08, ISO9022-11-special, MIL-STD 810G Method 502.5 I, MIL-STD 810G Method 501.5 I*
	Humidity	*100%, compliance with ISO9022-13-06, ISO9022-12-04 and MIL-STD 810G Method 507.5 I*
	Sealed against water, sand and dust	*IP68 according IEC60529 and MIL-STD 810G Method 506.5 I, MIL-STD 810G Method 510.5 I and MIL-STD 810G Method 512.5 I* *Protected against blowing rain and dust*

		Protected against temporary submersion into water (max. depth 1,4 m)
	Power Management	
	Supply voltage	*Nominal 12 V DC, Range 10.5 – 28 V DC*
	Internal power supply	*Removable & rechargeable Li-Ion battery, GEB212 2.6 Ah / 7.4 V*

[1] Measurement precision, accuracy, and reliability are dependent upon various factors including a number of satellites, geometry, obstructions, observation time, ephemeris accuracy, ionospheric conditions, multipath etc. Figures quoted assume normal to favorable conditions. Times required are dependent upon various factors including a number of satellites, geometry, ionospheric conditions, multipath etc. GPS and GLONASS can increase performance and accuracy by up to 30% relative to GPS only.

As mentioned before, the great advantage of using these instruments is common controller, in which with a use of one button surveyor may switch between GNSS antenna and total station interface. Thanks to motorization of the total station, it may move by itself combined with features like Automatic Target Recognition and LOCK. ATR is made for automatic aiming at the target, surveyor only roughly points on the target and the instrument finishes the rest finding the center of it. LOCK is the part of ATR allowing for continuous tracking the target, while it moves.

Total station Leica TS15 is also precise in its angle and distance measurements for every mode used. The table below displays characteristic of the instrument presented by the manufacturer on their website.

Table 4 - Characteristics of total station Leica Viva TS15. [http://www.leica-geosystems.com]

Angular Measurement	*Accuracy Hz, V[1]*	*2'' (0.6 mgon)*
	Display resolution	*0.1'' (0.1 mgon)*
	Method	*absolute, continuous, diametrical*
	Compensation	*Quadruple axis compensation*
	Compensator setting accuracy	*0.5'' (0.2 mgon)*
Distance Measurement	***Distance Measurement (Prism)***	
	Range[2]	
	Round prism (GPR1)	*3500 m (12000 ft)*
	3 Round prisms (GPR1)	*5400 m (17700 ft)*
	360° prism (GRZ4, GRZ122)	*2000 m (7000 ft)*
	360° mini prism (GRZ101)	*1000 m (3300 ft)*
	Mini prism (GMP101)	*2000 m (7000 ft)*
	Reflective tape (60 mm x 60 mm)	*250 m (800 ft)*
	Accuracy[3,4] / Measurement Time	
	Standard	*1 mm + 1.5 ppm / typ. 2.4 s*
	Fast	*2 mm + 1.5 ppm / typ. 0.8 s*
	Continuous	*3 mm + 1.5 ppm / typ. <0.15 s*
	Distance Measurement (Any Surface)	
	Range[5]	
	PinPoint R30 / R400 / R1000	*30 m (98 ft) / 400 m (1310 ft) / 1000 m (3280 ft)*

	Accuracy[3,6] / Measurement Time		
	PinPoint R30 / R400 / R1000	*2 mm + 2 ppm / typ. 3 s*	
	Distance Measurement (Long-range)		
	Long-range[2,4]	*>10000 m (>32800 ft)*	
	Accuracy[3,5] / Measurement Time		
	Long-range	*5 mm + 2 ppm / typ. 2.5 s*	
	General		
	Display resolution	*0.1 mm*	
	Shortest measurable distance	*1.5 m*	
	Method	*System analyzer based on phase shift measurement (coaxial, visible red laser)*	
	Laser dot size (Non-Prism)	*At 30 m: 7 mm x 10 mm, at 50 m: 8 mm x 20 mm*	
General	***Operation***		
	Sensitivity of Circular level	*6' / 2 mm*	
	Centering accuracy of Laser plummet	*1.5 mm at 1.5 m*	
	Number of drives	*1 horizontal / 1 vertical*	
	Environmental specifications		
	Working / Storage temperature range	*-20° C to +50° C / -40° C to +70° C*	
	Dust / water (IEC 60529) / Humidity	*IP55 / 95%, non-condensing*	
Motorization	*Rotation speed*	*45° (50 gon) / s*	
Automatic Target Aiming (ATR)	***Range***	***ATR Mode***	***Lock Mode***
	Round prism (GPR1)	*1000 m (3300 ft)*	*800 m (2600 ft)*
	360° prism (GRZ4, GRZ122)	*800 m (2600 ft)*	*600 m (2000 ft)*
	360° mini prism (GRZ101)	*350 m (1150 ft)*	*200 m (660 ft)*
	Mini prism (GMP101)	*500 m (1600 ft)*	*400 m (1300 ft)*
	Reflective tape (60 mm x 60 mm)	*45 m (150 ft)*	*–*
	Shortest distance to 360° prism	*1.5 m*	*5 m*
	Accuracy[1] / Measurement Time		
	ATR angle accuracy Hz, V	*1" (0.3 mgon)*	
	Base positioning accuracy	*±1 mm*	
	Measurement Time for GPR1	*3 – 4 s*	
	Maximum speed (Lock Mode)		
	Tangential (standard mode)	*5 m / s at 20 m, 25 m / s at 100 m*	
	Radial (tracking mode)	*4 m / s*	
	Searching		
	Search time in field of view	*Typ. 1.5 s*	
	Field of view	*1° 30' (1.66 gon)*	
	Definable search windows	*Yes*	
	Method	*Digital Image processing*	

[1] Standard deviation ISO 17123-3

[2] Overcast, no haze, visibility about 40 km; no heat shimmer

[3] Standard deviation ISO 17123-4

[4] To Round Prism GPR1

[5] Object in shade, sky overcast, Kodak Grey Card (90% reflective)

[6] *Distance >500 m 4 mm + 2 ppm*

Nowadays, GPS receiver and Total Station are basic equipment in every surveyor company. The better accuracy and precision the higher price, but sometimes surveyor can manage to increase the accuracy of measurement by improving the technology – a higher number of series or geometry of network, ratio between two next distances is not large.

Reflectorless total station (as the Leica TS15) can measure to any surface, so the points, which are hard to get on to put the reflector are now easy to measure. Of course, it is not as precise as measurements to a reflector, many factors are adding up to estimate the final precision of measured distance as well as if the measurement is possible or not. Author of the article 'Examination of range and accuracy of reflectorless distancers' [12] writes about how various factor influence the possibility of measuring a distance to any surfaces and their accuracy. Test was mainly conducted is laboratory conditions. Targeted surface had many different colors (white, grey, brown, black) and textures (reflective foil, aluminum foil, coarse-grained sandpaper, fine-grained sandpaper), angle of incidence of laser has been changed manually starting from right angle and changing it every 10gon on each step to reach angle equal to 20gon (30gon for longer distance – laser dot size occurred to be too big).

The analysis proves that the best results provide reflective foil and white targets, even for acute angles of incidence and long distances. Also, as expected, dark color targets and aluminum foil presented poor performance with bigger and bigger distances, for angles of incidence lower than 80gon the measurement was impossible. It is due to absorption and dispersion of laser beam. The interesting fact is that coarse-grained sandpaper and fine-grained sandpaper targets (imitating rough surfaces of a building) performed very successfully (at least one of tested laser range finders) for mid-range distances, but only with an angle of incidence close to right angle, in other cases the laser beam was dispersed and the measurement failed.

Next instrument from Leica Company is the Laser ScanStation C10. Thanks to this equipment the high definition surveying (HDS) is possible. Rotating laser scans the scene and obtains the dataset of angles and distances and then calculating plane and vertical coordinates, it also provides information about the intensity of laser reflections. These instruments help to acquire large dataset in very short time for better as-built or existing information. The measured is the whole scene or predefined fraction of it. If the scene is extensive we scan from multiple stations. Then it is possible to merge them with sufficient features overlap in post-processing.

Table 5 - Characteristics of laser scanner Leica ScanStation C10. [http://www.hds.leica-geosystems.com]

System Performance	*Accuracy of single measurement*	
	Position[1]	*6 mm*
	Distance[1]	*4 mm*
	Angle (horizontal/vertical)	*60 µrad / 60 µrad (12" / 12")*
	Modeled surface precision[2]*/noise*	*2 mm*
	Target acquisition[3]	*2 mm std. Deviation*
	Dual-axis compensator	*Selectable on/off, resolution 1", dynamic range +/- 5', accuracy 1.5"*
Laser Scanning System	*Type*	*Pulsed; proprietary microchip*
	Color	*Green, wavelength = 532 nm visible*
	Laser Class	*3R (IEC 60825-1)*
	Range	*300 m @ 90%; 134 m @ 18% albedo (minimum range 0.1 m)*
	Scan rate	*Up to 50,000 points/sec, maximum instantaneous rate*
	Scan resolution	*Spot size: from 0 – 50 m: 4.5 mm (FWHH-based); 7 mm (Gaussian-based)*
		Point spacing: fully selectable horizontal and vertical; <1 mm minimum spacing, through full range; single point dwell capacity
	Field-of-View	*Horizontal: 360° (maximum)*
		Vertical: 270° (maximum)
		Aiming/Sighting: parallax-free, integrated zoom video
	Scanning Optics	*Vertically rotating mirror on horizontally rotating base; Smart X-Mirror™ automatically spins or oscillates for minimum scan time*
	Data storage capacity	*80 GB onboard solid-state drive (SSD) or external USB device*
	Integrated color digital camera with zoom video	*Single 17° x 17° image: 1920 x 1920 pixels (4 megapixels)*
		Full 360° x 270° dome: 260 images; streaming video with zoom; auto-adjusts to ambient lighting
	Onboard display	*Touchscreen control with stylus, full color graphic display, QVGA (320 x 240 pixels)*
	Level indicator	*External bubble, electronic bubble in onboard control and Cyclone software*
	Data transfer	*Ethernet, WLAN or USB 2.0 device*
	Laser plummet	*Laser class: 2 (IEC 60825-1)*
		Centering accuracy: 1.5 mm @ 1.5 m
		Laser dot diameter: 2.5 mm @ 1.5 m
		Selectable ON/OFF
Environmental	*Operating temp.*	*0° C to 40° C / 32° F to 104° F*
	Storage temp.	*-25° C to +65° C / -13° F to 149° F*
	Lighting	*Fully operational between bright sunlight and complete darkness*
	Humidity	*Non-condensing*
	Dust/humidity	*IP54 (IEC 60529)*

[1] *At 1 m – 50 m range, one sigma*

[2] *Subject to modeling methodology for modeled surface*

[3] *Algorithmic fit to planar HDS targets*

Nowadays, more and more common are unmanned aircraft vehicles using as an equipment for mapping or surveying. The range of application is tremendous, the author tried to check if a commercial drone is capable of dealing with accurate land surveying work. Used equipment for this task is DJI Phantom 3 Professional. The table below presents a brief introduction to this model.

Table 6 - Characteristics of drone DJI Phantom 3 Professional. [http://www.dji.com]

Aircraft	*Weight (including battery and propellers)*	*1280 g*
	Diagonal Size (Excluding Propellers)	*350 mm*
	Max Ascent Speed	*5 m/s*
	Max Descent Speed	*3 m/s*
	Hover Accuracy	*Vertical: +/- 0.1 m (when Vision Positioning is active) or +/- 0.5 m*
		Horizontal: +/- 1.5 m
	Max Speed	*16 m/s (ATTI mode, no wind)*
	Max Service Ceiling Above Sea Level	*6000 m (Default altitude limit: 120 m above takeoff point)*
	Operating Temperature	*0°C to 40°C*
	GPS Mode	*GPS/GLONASS*
	Max Flight Time	*Approx. 23 minutes*
Gimbal	*Controllable Range*	*Pitch -90° to +30°*
	Stabilization	*3-axis (pitch, roll, yaw)*
Remote Controller	*Operating Frequency*	*2.400 GHz-2.483 GHz*
	Max Transmission Distance	*Up to 5 km or 3.1 miles (unobstructed, free of interference) when FCC compliant*
		Up to 3.5 km or 2.1 miles (unobstructed, free of interference) when CE compliant
	Operating Temperature	*32° to 104° F (0° to 40° C)*
Camera	*Sensor*	*Sony EXMOR 1/2.3" Effective pixels: 12.4 M (total pixels: 12.76 M)*
	Lens	*FOV 94° 20 mm (35 mm format equivalent) f/2.8, focus at ∞*
	ISO Range	*100-3200 (video)*
		100-1600 (photo)
	Shutter Speed	*8s -1/8000s*
	Image Max Size	*4000 x 3000*
	Still Photography Modes	*Single Shot*
		Burst Shooting: 3/5/7 shots
		Auto Exposure Bracketing (AEB): 3/5
	Video Recording Modes	*UHD: 4096x2160p 24/25, 3840x2160p 24/25/30*
		FHD: 1920x1080p 24/25/30/48/50/60
		HD: 1280x720p 24/25/30/48/50/60
	Supported SD Card Types	*Micro SD*
		Max capacity: 64 GB. Class 10 or UHS-1 rating required
	Max Video Bitrate	*60 Mbps*
	Supported File Formats	*FAT32 (≤ 32 GB); exFAT (> 32 GB)*
	Operating Temperature	*32° to 104° F (0° to 40° C)*
	Photo	*JPEG, DNG*
	Video	*MP4, MOV (MPEG-4 AVC/H.264)*

Presented drone has a big drawback which is a strict integrity between its parts. It is impossible to change the sensor mounted on gimbal. Otherwise that would cause damage to the whole equipment. According to Polish regulations about the classification of airships [2], UAVs cannot have bigger or equal maximum take-off mass (MTOM) to 25kg. This unmanned aerial vehicle, according to classification presented by Henri Eisenbeiss [5], is the type of mini and micro and its carrying capability cannot be higher than 5 kg. That kind of light airships are not resistant to wind gusts. The airy construction may yaw from the planned trajectory.

The market is full of various drones, some are adjusted to even work in different environments like under the water. But here we would like to focus on aerial units. Well-known in land surveying field company Trimble has in their offer one rotary wing and two fixed-wings drone. The manufacturer says that one of the fixed-wings (UX5 HP) is able to obtain data with high spatial precision, thanks to integrated GNSS system and PPK (Post-processed Kinematic). The great advantage of this is no need to measure any Ground Control Points (GCPs), which shorten field work to a minimum.

For task presented in the thesis, the drone had to do oblique photos. It is impossible to achieve with fixed-wing drones. The choice came down to mentioned DJI Phantom 3, it is due to its availability, ease of operating, performance and price.

3.3. First measurement day

At the date of 5th February 2016, field work started with the investigation of the measurement site. Tripods were set up on future total station position. Because of winter time during conducting the survey process, there was a need to clear of the snow from surroundings of the station and let the tripod for a while to reduce any future movements related to melting snow and ice under the pressure. Next step was to tie all forthcoming measurements to the Norwegian Coordinate System EUREF89-UTM-zone32 with vertical datum NN2000. This process started with calculating spatial coordinates of the first station using intersection and integration of the GNSS antenna with a 360 degrees reflector on the same pole. The GPS points were measured using Real-Time Kinematic mode, which allows getting coordinates with correction at the site. After 10 measurement epochs (1Hz), the distance and angles from the total station were measured to the reflector on the pole. According to this process, three GPS points were measured to obtain enough observation (plus additional observation for calculating a standard deviation of setting up coordinates) to let the program determine the spatial position of the total station.

Later on, coordinates of two other stations were calculated from the tied up station. On the spots of total stations were tribraches with reflectors. Surveyors did not perform the stabilization of any point in the terrain, so after the Leica Viva TS15 was set up, all angular measurements were conducted for the double-edged method in both faces and two series. Prepared field sheets may be found in Appendix 1 – 'Field sheets'. Simultaneously, laser scan station was set up and few HDS targets – 6-inches circular plane targets on tripods – successively scanning the southern part of the tower.

Scanning process itself always started with pre-scan on a medium density of the whole scene. After that from the scanned scene were selected the object of interest and some surrounding features for forthcoming cloud-to-cloud registration in post-processing. They were scanned with the highest quality and density. The time of scan process depends on the range and quality acquired scenes.

The weather conditions did not let to try flying with the UAV, the wind blew too strong. That is why the second day of measurement day was required.

Figure 10 - Selected, observed levels on the tower from the angular method. Levels from 3 to 8 are located right under the standings and main gallery.

3.4. Second measurement day

On the 9th February, the second day of measurement was conducted. Author planned the second field work in similar, as the first one, atmospheric conditions, but with a lighter wind to be able to fly with UAV.

Surveyors started with finishing up the laser scanning process. During the first day, the tower was measured from 4 scan stations covering mainly the southern part. The laser scanning process during the second day was performed without reference to the Norwegian Coordinate System. There were just scans in a local coordinate system, the plan was to stitch the both days with a cloud-to-cloud registration. Some nearby features were scanned with high density same as during the first day.

The acquisition of photos using the DJI Phantom 3 Professional was executed taking oblique photos flying around the object from a safe distance. To do so UAV operator came close with the drone to the tower set location as a point of interest, then he flew away from the object and ordered the unit to do the whole circle while the operator was snapping pictures manually. The flaw of this procedure is different distances between the drone and the object resulting in uneven scope on the picture, which also mean that the Ground Sample Distance (GSD) differs. (By using word 'ground' in GSD, the author means the distances on the object representing one pixel on the photo.)

Overall, 150 pictures were taken using the drone at a level of 6 different heights. The operator tried to maintain high overlap between taken photos. The overlap between rows and pictures in a row was over 80%.

4. Post-processing

Data acquired during field work have to be processed to obtain results interesting for the inventory of the object, some methods give results at the site – closer presented in previous chapter "Methods".

Network adjustment is usually the very first step during post processing, it is because obtained data and measurements are imprecise to a certain extent and this process let surveyors know how good the network is, what the errors are at stations, what the quality is of measurements.

Table 7 - Network stations' coordinates and their standard deviations

Point ID	North [m]	Std. N [m]	East [m]	Std. E [m]	Height [m]	Std. H [m]
S1	7 033 320.835	0.004	571 384.183	0.004	120.358	0.003
S2	7 033 421.354	0.006	571 324.786	0.008	115.971	0.005
S3	7 033 365.606	0.018	571 566.102	0.005	109.913	0.004

As the reader may notice, the network looks very good, with one exception. The standard deviation for north coordinate in station S3 is rather big, almost 2 cm. The reason for this might be only one series, instead of two, on this station, due to surveyor's tiredness and inattention.

Accuracy analysis provides also information about ellipse errors for each station, a- long axis, b- short axis and φ- azimuth to the long axis. The table below presents there parameters for this case.

Table 8 - Ellipse error's parameters for 3 network stations

Point ID	a [m]	b [m]	(φ) [g]
S1	0.018	0.005	192.9
S2	0.008	0.005	69.6
S3	0.005	0.003	34.7

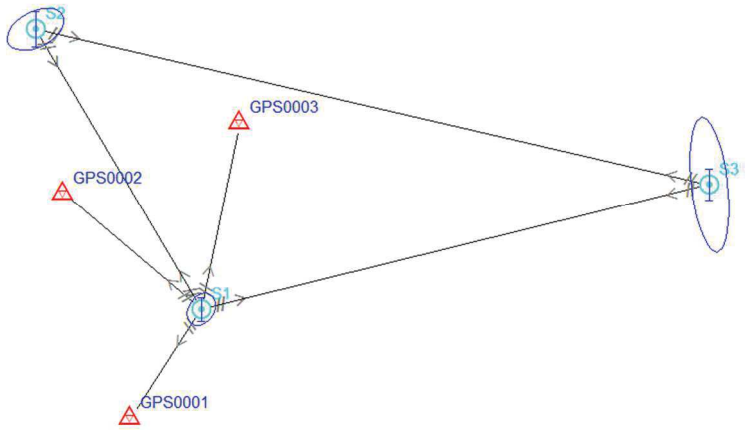

Figure 11 - Presentation of ellipse errors on the stations.

Both tables above are parts of the network adjustment report (Appendix 2 – 'The network adjustment report').

4.1. Calculating inclination of the tower from angular observations

The first step to obtain the inclination of the tower is calculating coordinates of stations and the object (its vertical axis). Coordinates were calculated using Gemini Oppmåling software, table below presents results.

Table 9 - Coordinates of stations and the axis of the tower.

point	X [m]	Y [m]	Z [m]
S1	7033320.835	571384.183	120.358
S2	7033421.354	571324.786	115.971
S3	7033365.606	571566.102	109.913
TT	7033447.225	571477.024	-*

** - different levels were measured*

From conducted at site measurements concerning inclination of the tower, the author created field sheets which can be found in the Appendix 1 - 'Field sheets'.

The table below presents a list of a plane and vertical direction from 2 series and three stations.

Table 10 - Mean horizontal and vertical angles from 2 series at 3 stations.

	Station 1		Station 2		Station 3	
Target	Plane [g]	Vertical [g]	Plane [g]	Vertical [g]	Plane [g]	Vertical [g]
LP1	38.9196	97.3887	87.8440	95.5752	345.2697	90.9412
LP2	38.9268	93.6184	87.8486	91.8278	345.2705	86.0988
LP3	38.9205	90.8190	87.8424	88.9311	345.2710	82.9366
LP4	38.9207	87.6835	87.8408	85.7119	345.2691	79.0170
LP5	38.9249	84.6149	87.8407	82.6184	345.2714	75.3613
LP6	38.9354	81.5913	87.8402	79.5690	345.2774	71.8116
LP7	38.9424	78.6536	87.8344	76.6190	345.2867	68.4750
LP8	38.9462	76.8974	87.8463	75.0341	345.2864	66.5255
RP1	41.8408	97.3649	90.8055	95.5728	349.0693	91.0500
RP2	41.8460	93.8441	90.8070	91.6479	349.0758	86.1237
RP3	41.8356	90.8135	90.8010	88.9365	349.0770	82.9002
RP4	41.8358	87.6622	90.7960	85.7412	349.0817	79.0223
RP5	41.8364	84.5768	90.7908	82.7335	349.0875	75.2943
RP6	41.8424	81.5461	90.7852	79.6685	349.0999	71.7751
RP7	41.8504	78.5858	90.7851	76.6143	349.1133	68.3877
RP8	41.8539	76.8869	90.7997	75.0176	349.1159	66.5456

In next step, author calculated average heights of observed profiles of the tower and reduced to the most bottom profile, as well as reduced plane directions to the bottom left one from every measuring station. Results are presented in the table below.

Table 11 - Horizontal angles reduced to the left bottom observation.

profile	Height [above the first section]	S1		S2		S3	
		1L	1R	2L	2R	3L	3R
1	0.0	0.0000	2.9213	0.0000	2.9615	0.0000	3.7996
2	9.3	0.0073	2.9265	0.0046	2.9631	0.0008	3.8061
3	16.2	0.0009	2.9161	-0.0016	2.9570	0.0014	3.8073
4	24.3	0.0012	2.9163	-0.0032	2.9520	-0.0006	3.8121
5	32.2	0.0053	2.9169	-0.0033	2.9468	0.0017	3.8178
6	40.3	0.0158	2.9229	-0.0038	2.9413	0.0077	3.8302
7	48.4	0.0228	2.9309	-0.0096	2.9411	0.0170	3.8437
8	53.0	0.0266	2.9343	0.0023	2.9557	0.0167	3.8462

After preparation of all, author calculated mean values of direction for each observed section, these values represent direction to the vertical axis of the tower for a particular section.

$$k_j^i = \frac{kL_j^i + kR_j^i}{2}$$

where:

kL_j^i - plane direction from j-th station to left edge of i-th profile

kR_j^i - plane direction from j-th station to right edge of i-th profile

Table 12 - Average directions.

section	S1 [g]	S2 [g]	S3 [g]
1	1.4606	1.4808	1.8998
2	1.4669	1.4838	1.9034
3	1.4585	1.4777	1.9043
4	1.4587	1.4744	1.9057
5	1.4611	1.4718	1.9098
6	1.4693	1.4687	1.9190
7	1.4768	1.4658	1.9303
8	1.4805	1.4790	1.9314

Upon that, taking the first section as the reference, observed angles were calculated using following formula:

$$\Delta\alpha = k_j^i - k_j^1$$

where:

k_j^i - average direction from j-th station to i-th section

k_j^1 - average direction from j-th station to the first section

Table 13 - Observed angles on 3 stations.

section	St1 [g]	St2 [g]	St3 [g]
1	0.0000	0.0000	0.0000
2	0.0062	0.0031	0.0036
3	-0.0021	-0.0030	0.0045
4	-0.0019	-0.0064	0.0059
5	0.0004	-0.0090	0.0099
6	0.0087	-0.0120	0.0191
7	0.0162	-0.0150	0.0305
8	0.0198	-0.0017	0.0316

Based on the coordinates of stations and center of the tower, azimuths and distances from each station and the tower were calculated.

Table 14 - Azimuths and distances from station to the tower.

	from S1 to TT	*from S2 to TT*	*from S3 to TT*
dy [m]	*92.8408*	*152.2378*	*-89.0782*
dx [m]	*126.3896*	*25.8706*	*81.6186*
ϕ [g]	*40.33281*	*89.28394*	*52.78032*
Az [g]	*40.33281*	*89.28394*	*347.2197*
D [m]	*156.8239*	*154.4203*	*120.8161*

Next step was calculating component parts of inclination of the tower (ωx and ωy) using least mean square method (LMS method). Observation equation has the form:

$$v_{\alpha i}^{j} = -\frac{sinAz_j}{Dj} \cdot \rho \cdot \omega_{xi} + \frac{cosAz_j}{D_j} \cdot \rho \cdot \omega_{yi} - \alpha_{obs_i}^{j}$$

where:

Az_j – azimuth from j-th station to the center of the object,

D_j – distance from j-th station to the center of the object,

ω_{x/y_i} – component part of the inclination of the object along X/Y-axis,

$\alpha_{obs_i}^{j}$ – observed angles from j-th station to i-th section.

If the distances from stations to the center of the tower differed much, we would use the weight for the observations using the inverse of the square of the length in kilometers. However, this is not the case here.

Algorithm was conducted in matrix form using calculation program Microsoft Excel, factors matrix (A), vectors of absolute terms (L_1-L_8) and results (X_1-X_8) –vectors of component parts of inclination of the object are presented as follow:

A

-0.240322	*0.327165*
-0.406437	*0.069068*
0.388510	*0.355975*

L1	*L2*	*L3*	*L4*	*L5*	*L6*	*L7*	*L8*
0.0000	*0.0062*	*-0.0021*	*-0.0019*	*0.0004*	*0.0087*	*0.0162*	*0.0198*
0.0000	*0.0031*	*-0.0030*	*-0.0064*	*-0.0090*	*-0.0120*	*-0.0150*	*-0.0017*
0.0000	*0.0036*	*0.0045*	*0.0059*	*0.0099*	*0.0191*	*0.0305*	*0.0316*

$$X_i = (A^T A)^{-1} \times A^T L_i$$

Table 15 - Calculated component inclinations from angular measurements.

	X1	X2	X3	X4	X5	X6	X7	X8
ω_X [m]	0.0000	-0.0049	0.0092	0.0141	0.0189	0.0245	0.0326	0.0159
ω_Y [m]	0.0000	0.0155	0.0017	0.0025	0.0104	0.0338	0.0591	0.0718

From component parts of the inclination were calculated the resultant inclinations and their azimuths.

$$\omega_i = \sqrt{\omega_{X_i}^2 + \omega_{Y_i}^2}$$

$$Az_\omega = arctg(\frac{\omega_Y}{\omega_X})$$

Next step covered accuracy analysis of calculated component parts of the inclination for each section. Coming formulas were used for every observation level:

$$v_i = AX_i - L_i$$

$$m_{0_i} = \sqrt{\frac{\sum v_i^2}{n-u}}$$

$$\delta_{\omega_X} = \pm\sqrt{Cov(X)_{[1,1]}}$$

$$\delta_{\omega_Y} = \pm\sqrt{Cov(X)_{[2,2]}}$$

where:

n – number of observations

u – number of unknowns

$Cov(X)_{[1,1]}$ – element in 1st row and 1st column in covariance matrix

$Cov(X)_{[2,2]}$ – element in 2nd row and 2nd column in covariance matrix

Having already the component parts of inclination, we may have calculated the generalized inclination, showing the leaning of the tower in units m/m (for instance 0.005m/m is 5 millimeters

for each 1 meter of height), to do so we need heights of the observed profiles and calculated component parts.

$$X_{ex/ey} = (H^T H)^{-1} H^T L_{ex/ey}$$

where:

H – vector of heights of the observed profiles

$L_{ex/ey}$ – vector of calculated component parts of inclination along X/Y –axis

Table below presents results of calculation.

Table 16 - List of results from angular measurements.

profile	ω_x *[m]*	$\delta\omega_x$ *[m]*	ω_y *[m]*	$\delta\omega_y$ *[m]*	ω*[m]*	Az_ω*[g]*	e_x *[m/m]*	e_y *[m/m]*
1	*0.0000*	*0.0000*	*0.0000*	*0.0000*	*0.0000*	*0.0000*	*0.00051*	*0.00098*
2	*-0.0049*	*0.0000*	*0.0155*	*0.0000*	*0.0162*	*119.5347*		
3	*0.0092*	*0.0014*	*0.0017*	*0.0017*	*0.0094*	*11.9044*		
4	*0.0141*	*0.0019*	*0.0025*	*0.0023*	*0.0025*	*11.1919*		
5	*0.0189*	*0.0046*	*0.0104*	*0.0058*	*0.0216*	*31.8428*		
6	*0.0245*	*0.0101*	*0.0338*	*0.0127*	*0.0417*	*60.0298*		
7	*0.0326*	*0.0134*	*0.0591*	*0.0167*	*0.0675*	*67.9619*		
8	*0.0159*	*0.0005*	*0.0718*	*0.0006*	*0.0735*	*86.1175*		

In presented above method, based on measuring very small angles (Δα), coordinates of stations may be determined by loose quality of the network – about +/- 1 meter. [8].

In conclusion, the inclination of the tower is rather small. Generalized inclination of the object is 0.027m on X-axis and 0.052m on Y-axis for 53-meter cylinder. Accuracy analysis indicates that observed level 6 and 7 are measured with rather poor quality, due to over 1cm standard deviation on both component parts of inclination. The tower successively is leaning towards east (starting from the north at lower levels), with one exception at the second observed level, where the azimuth is indicating south direction (about 120 gons).

In Appendix 3 - 'Inclinations from angular observations' graphical visualization is presented of component parts of inclination and generalized ones in three different planes XY, XZ and YZ.

4.2. Computing 3D point cloud from pictures

The captured photos with the help of DJI Phantom 3 Professional were processed in software Pix4D mapper. Author's knowledge about expected result of processing photos was rather vague, so the short investigation was conducted.

The software offers many different set ups for computing point cloud. Basic knowledge of the photogrammetry and the software is obligatory. The work in Pix4D in our case consists of 3 major steps:

- Initial processing,
- Geolocation and reoptimize,
- Computing 3D point cloud and mesh.

Initial processing is also a more complex process. It all starts with keypoints extraction, whereas the program picks an interesting area with decent contrast. Software lets users select from many option in terms of what scale of the photo should be processed before the actual extraction. Users can select from:

- 2 (Double image size) – recommended for small images, to extract more features as well as increase the overall accuracy.
- 1 (Default image size) – as name suggest this mode is recommended by default for extracting keypoints.
- ½, ¼, ⅛ (Fraction image size) – the lower fraction is the faster process works and less features can be extracted. Recommended for blurry photos or very large ones.

It is a good idea to perform the initial processing using one of the fraction image size, if the sufficient amount of keypoints will be found user may be sure that there will be also enough using default mode, but processing time is reduced by a great deal. This can be used at the site, to quickly check if the captured pictures will provide sufficient amount of keypoints.

Matching process's options allow users to pick how the pictures were captured. There are Aerial Grid or Corridor, Free flight of Terrestrial and Custom mode. Basically, it tells the software how it should choose neighboring photos. One more option is available 'Use Geometrically Verified Matching', it slows the process, but also make it more resistant to errors. It takes into account the relative camera positions (not only the image content) letting avoid incorrect matches, for example, the repetitive content of photos- like windows on the building's façade.

The last component of the initial processing is the calibration. The user may select how many keypoints will take part in this process by setting automatic or selecting a maximum number of keypoints to be extracted per image. The second option is very useful for very large photos, letting the process to be performed faster than automatic, but equally accurate. The user may also choose what parameters should be calculated, this is by default set for 'All' and it is recommended to be like that, with an exception for highly professional photogrammetric cameras with known internal parameters.

Improving geolocation and re-optimization is the next major step. In initial processing the results are tie points in, selected in the project properties, coordinate system. Having the ground control points measured on the tower, the user may improve the geolocation accuracy. Preliminary geolocation of the project is acquired from geotags of pictures depending on how accurate GPS location is provided by the UAV.

To improve the geolocation and accuracy of the whole project, author measured GCP on the tower using the total station during the field work on the first measurement day. Most of them are on the upper part of the tower and these are the vertexes of the main gallery, and some additional points were measured on the cylinder, easily distinguished.

In Pix4D mapper it is possible to manually type in the names and coordinate of the GCPs, but also the uploading text file with name, X, Y and Z coordinates. It is important to set the same coordinate system as the project has. Next step is pointing the selected GCP at the photos, there is also two-way for doing this step. First of them is selecting pixels representing on the photos in basic view, so the user should know at what pictures the GCP is visible. Second method is with use of rayCloud (initial processing step is required for this approach), software shows pictures where the point is represented. After the user pointed several GCPs, the whole project should be re-optimized. Thus, it gains new, more accurate geolocation.

The last step is creating the 3D point cloud and mesh. The software allows using different settings for processing. The most important one is point cloud densification option where the user can select 'Image scale' which corresponds to a scale of the image at which additional 3-dimensional points are computed. Also, the important setting is 'point density'. This parameter defines how many point per area unit are going to be computed. Last, but not least is 'Minimum Number of Matches' this is the minimum number of valid re-projections of the point to be represented in 3D point cloud. The author does not need the meshes as an output, so those settings will not be provided here.

The author's personal experience with the software is faint. Thus, short point clouds processing analysis was conducted. The main idea was to create few point clouds with different settings. The contradistinction in settings is 3-level. The levels are: how many photos are taken into the processing, are the pictures original or edited and is the point cloud computed by slow or default processing.

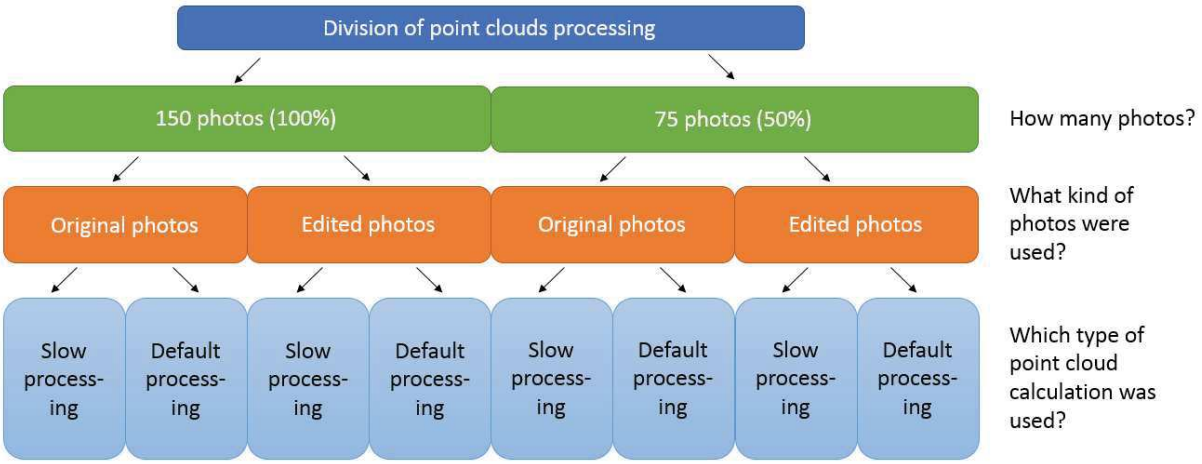

Figure 12 - Scheme for creation of several point clouds using photos captured by UAV.

8 different point clouds were computed. They differed one from another in quality and density. All of them were computed using the setting 'Minimum Number of Matches' equal to 3. Description of visual evaluation of the tower was performed in matters like noises, density, coverage of the main gallery, coverage of the cylinder, shape of the cylinder and additional comments.

Description of computed point clouds:

- 150 photos (100%)
  - Original photos
    - Default processing

- The point cloud was characterized by noises in an upper part of the tower. After cleaning process, a number of points in the dataset was 1.7 million. The density is rather good. The coverage of the cylinder is good with an exception in the north part, less lit, where the point cloud density is noticeably lower. Some cross sections were selected to analyze the cylinder, in visual evaluation the object was not a closed figure, and a fitted sphere into these datasets was characterized in root mean square (RMS) error from 3- 5 cm. The prism was covered in 100 per cent, the roof was displayed well, and better density and less of noises were over the sunny side.

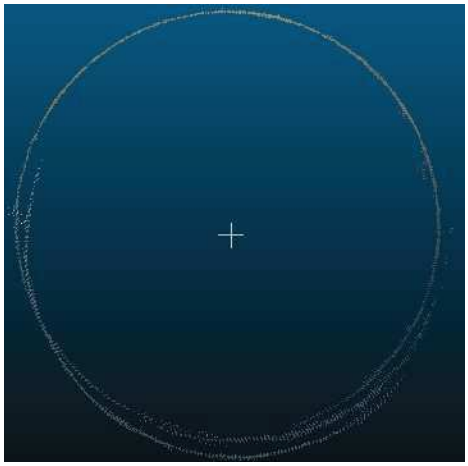

Figure 13 - Selected cross section of the tower, presenting the not closed figure of the cylinder.

- Slow processing

  The point cloud was characterized by high density, over 21 million points, subsampling is advised, because there is no reason to have so dense dataset, and it should improve the working smoothness. The noises were located were close to the elements on the tower, these noises were also very dense. The coverage of the cylinder was not full, at the bottom was a big blank spot with size around 9 x 3.5 meters. The prism and roof were depicted very well with decent coverage, removed noises were located away from the sunny side. Cross sections selected on the cylinder did not present a closed figure, and fitted spheres into cross sections had RMS error in the range of 6-9 cm. Moreover, the radius of the spheres differed a couple of centimeters.

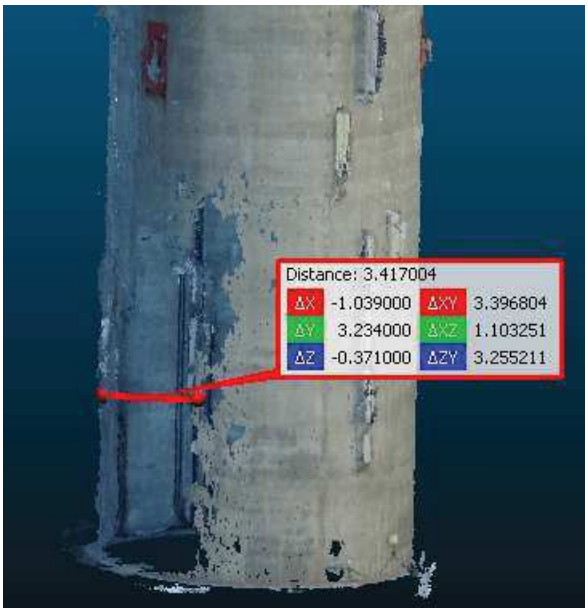

Figure 14 - Missing part of the object in the dataset.

  - Edited photos
    - Default processing

The point cloud was characterized by a vast range of noises, around the tower. The density is rather good. After removing noises and elements which are not analyzed in the thesis, the amount decreased from 2.7 to 1.7 million points. The cylinder was covered in total, even the north part had more computed points than the same part in default processing with original photos. The main gallery and the roof are also very well depicted using this set of options. The elements and their supports are easily distinguishable. The cylinder's cross sections made a closed figure with just a slight noises – some points were 'inside'. The RMS errors computed after fitting the sphere into few selected cross sections varied from 1 to 5 cm

Figure 15 - Prism and roof, depicted using all edited photos in default processing. White pixels are not removed noises.

- Slow processing

  The point cloud was very dense, a number of points after removing unnecessary parts and noises was 21.8 million. Highly recommended was subsampling the dataset for keeping the process smoother. Noises very close to the tower, mostly near metal components. The density of dataset looked rather even. Moreover, the recommended subsampling could make the points' distances equal to set value. The cylinder was covered in the whole surface of it, and selected cross sections showed that it made a closed figure. After fitting the spheres into cross sections, the differences between radiuses were about 1 cm, and the RMS of fitted figures was from 2 to 3 cm. The main gallery and roof were displayed very well, and with noises close to it.

Figure 16 - Noises around the tower. They are concentrated on the metal shining parts.

- 75 photos (50%)
  - Original photos
    - Default processing

      As expected, the point cloud was very poor. The number of points after removing all noises and not analyzed parts had 270 thousand. The dataset was characterized by many parts not covered by points at all. The estimated coverage was 60 percent on the cylinder and about 20 percent on the main gallery. Moreover, the prism was split into two parts, one from another was translated about 2.8 meters in height coordinate. Noises were not very extensive, very close to the tower and in few number. The cross sections analysis showed that computed points were far from closed figure, so fitting sphere into them had no meaning. Many elements located on the tower (radio- and TV-transmitters) were not computed, even if they were, the quality and density were very low.

Figure 17 - Split prism, the break line goes through the differences in a lightening of the object.

    - Slow processing

      The quality of the tower was not improved comparing to the default processing, with the same quantity and type of photos. The coverage of the cylinder was estimated for about 40%, and the prism - less than 20%. The tower was still split into two parts, which were translated one from another about 1.7 meters. The noises were only on the east and west side of the tower, this was also the place of the break the object into two parts- along the Z-axis. The parts which were presented in the dataset were very dense. Only 30-35% of the whole tower were presented by 2.7 million points. The lack of coverage and division of the tower made cross sections analysis futile and insignificant.

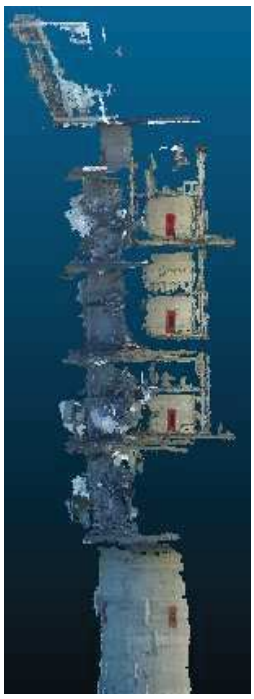
Figure 18 - Overall view for dataset made of half of the taken, original photos in slow processing mode.

  - Edited photos

- Default processing

  The point cloud was characterized by very good coverage, despite some small blank spots between the support constructions for radio- and TV-transmitters. Noises were noticed only in the upper part of the tower with a close range from it, and also at the west and east side. The number of points after cleaning process was 1.0 million, which is much less than in the point cloud with the same setting, but 150 photos. The cross sections' analysis presented the cylinder as a closed figure on the entire height of the object. Fitted spheres showed that radius sizes differed for less than 1cm, and RMS error did not exceed 2.2cm. The main gallery and roof were displayed very well. Clearly, the sunny part of it was denser.

Figure 19 - Missing parts of the cylinder near support constructions.

- Slow processing

  The object with this setting was characterized by very high density, after removing noises, 12.5 million of points (comparing to 1.0 million points in default processing). The subsampling was recommended, in order to work more smoothly in software. Noises were dense and located in upper part of the tower, very close to it, and mostly on the west and east side. The cylinder is covered in 90%, some small blank spot could be noticed near the support constructions for radio- and TV-transmitters, as well as a big gap in the dataset at the bottom of it. The size of the hole was about

Figure 20 - Highly dense point cloud. The roof is badly depicted.

10 x 3 meters. The main gallery was depicted very well, but the roof was only presented from the southwest side. Cross section analysis showed a closed figure. Fitted spheres revealed that difference between radiuses was about 2cm, and the RMS errors were around 2.5cm

By edited photos, the author has in mind that for the better pixel identification, the exposure of pictures taken from the north side of the tower was increased to allow Pix4D mapper extract more 2D keypoint matches for a single photo. The modification was performed in Adobe Photoshop Lightroom, using free trial version. Unfortunately, the geotags (conjugate locations of taken pictures), which provides GPS mounted in the UAV DJI Phantom 3 had been changed due to a usage of the picture editing software. It is because the software cannot export pictures with geotags with sufficient accuracy, so some of valid information were lost.

Fortunately, Pix4D mapper may manage with this problem only by setting the accuracy of geotags onto low. The process with use of the GCPs on the tower will reposition the conjugate locations into the correct place, making the vectors from an initial position to computed position very long. It usually takes more time to correctly process edited photos.

The table below presents the time needed to finish component of the whole process in Pix4D mapper. The hardware specifications are: Intel ® Core ™ i3 CPU, 8GB of RAM memory and 64-bit Operating System.

Table 17 - Time of processing for different setting of Pix4D mapper and different computation processes.

	150 photos				*75 photos*			
	original photos		*edited photos*		*original photos*		*edited photos*	
	default processing	*slow processing*	*default processing*	*slow processing*	*default processing*	*slow processing*	*default processing*	*slow processing*
1)	*32m:32s*	*32m:32s*	*45m:56s*	*45m:56s*	*9m:49s*	*9m:49s*	*17m:26s*	*17m:26s*
2)	*3h:49m:33s*	*8h:55m:33s*	*58m:26s*	*5h:58m:56s*	*11m:31s*	*34m:34s*	*1h:24m:18s*	*2h:31m:04s*
3)	*14m:50s*	*37m:50s*	*31m:06s*	*1h:40m:29s*	*3m:34s*	*13m:42s*	*21m:51s*	*23m:39s*

1) Initial processing

2) Point Cloud Densification

3) 3D Textured Mesh Generation

As it was said, time needed for Initial Processing to compute edited photos is longer than in case original photos, due to lost accuracy using Adobe Photoshop Lightroom. Time to process point cloud densification is expanding either for the different type of processing or the different type of photos. The exception in given times is process worked on original 150 photos, it is because

of the range of processing. Just in that case the user did not set the processing area, so the software computed points for the whole scope of the pictures, which eventually took more time. In any other cases, the processing area was set on the tower. The 3D textured mesh generation also shows similar tendency between processing setting and types of used photos.

As the conclusion, different settings give different results for this particular project, 75 photos had simply not enough overlap between neighboring pictures to obtain sufficient point cloud, even though the datasets from edited photos in both processing settings presented the whole tower as one object (no split, like using original pictures), some parts were missing. To avoid that, it was better to use all taken pictures for computation. It is easy to notice that, the datasets look better for edited pictures rather than original. Even though the point clouds were denser and with better coverage using the photos with increased exposure, this approach has raised the question: what is the quality of 'artificially' created points. Comparing point clouds created from original and edited photos (with same processing mode- default processing), the calculation of distances were performed and the following results showed up.

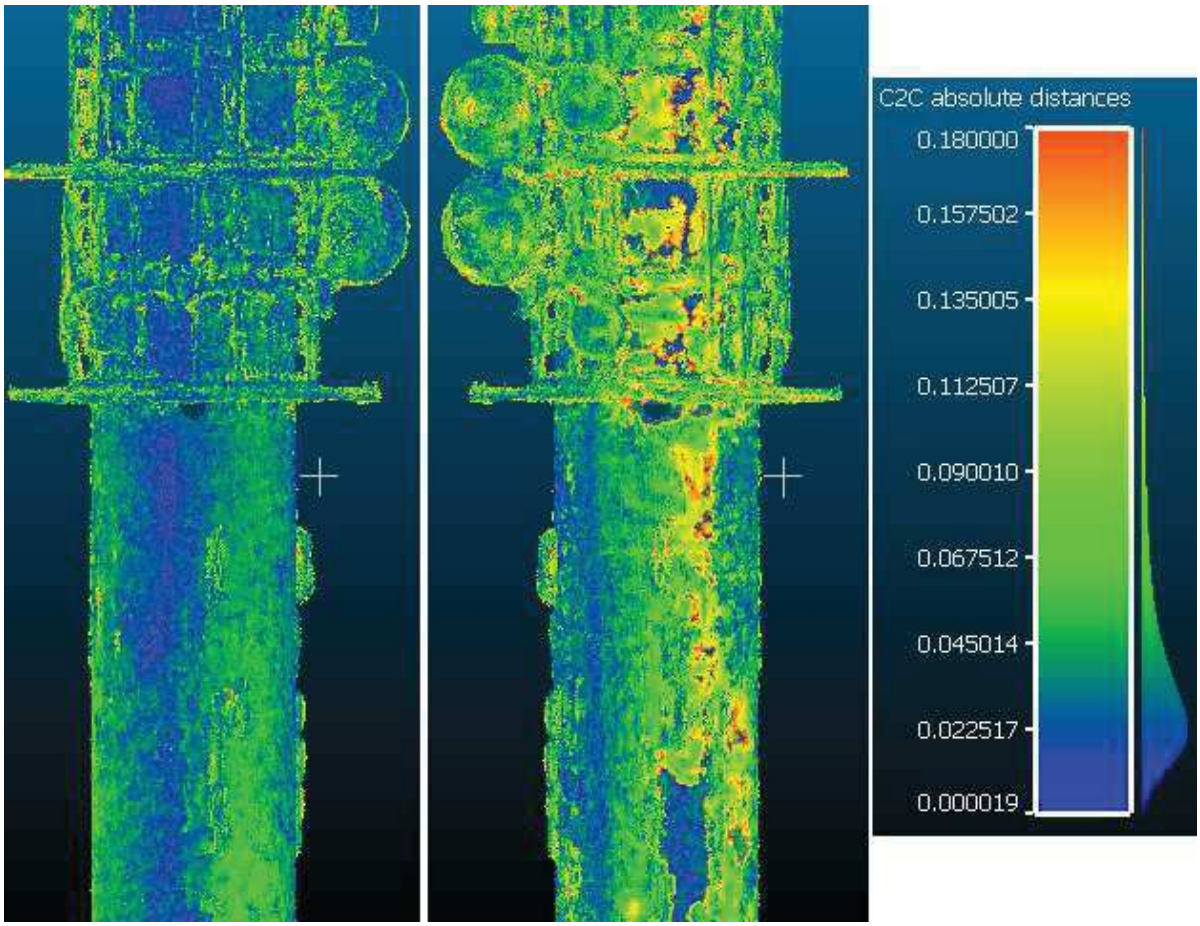

Figure 21 - Cloud to cloud distances. Reference: point cloud made of original photos, Model: point cloud made of edited photos.

Figure 21 shows the distances between two point clouds, two sides of the cylinder are showed, on the left one there is south side – sunnier, on the right is north side of the tower- darker one. Distances computed shows the connection between accuracy and the lighting of the pictures used, tendency showed on figure 21 kept for the whole height of the tower. As a reminder, the cross sections in point cloud created using original photos did not make a closed figure, there were some gaps at the darker side of the cylinder. Thus, we may assume that the points created using edited pictures are characterized by higher accuracy.

Differences in chosen processing modes revealed that the result dataset is bigger, but not necessarily with better accuracy. The visual observation indicated that the coverage for slowly processed point clouds is smaller, so that may indicate the improvement of other computed points. A short comparison of two processed point clouds may give us few clues.

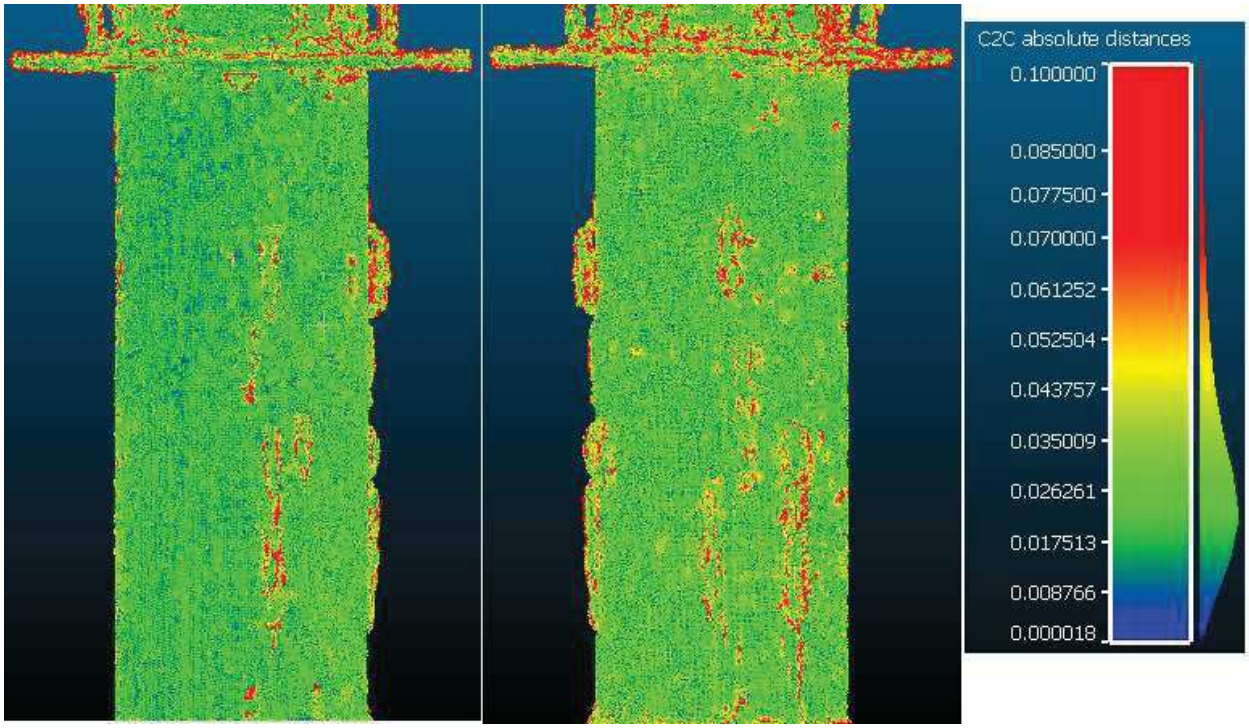

Figure 22 - Comparison of processing mode. On the left south side of the tower, on the right north side.

The green and blue color show in turns, which may be an indication of only denser model's point cloud. Although the accuracy and quality of computed points may differ a little bit from the default processing. The actual improvement may be noticed in cross sections analysis, which said that the differences radiuses of fitted spheres are smaller and the root mean square errors varies less than from the default processing mode. The red pixels are probably not removed noises around features mounted on the tower.

The different in processing time between original photos and edited ones for initial processing is almost imperceptible. Of course, we must take into account that pictures had to be edited, and time spent for it depends on the amount of them, as well as user's expertise and software literacy.

From gathered experience and visual observation, the last, ninth, point cloud was created using all edited photos which were processed in default mode, but with an exception that 4 (not 3, as previously) number of matches were required, this was aimed at reducing noises and probably increasing the quality of computed points. The report from the computation may be seen in Appendix 4 – 'Pix4D mapper – final point cloud's report'. This last computed 3D point cloud was the one used for further studies and analysis. Comparing it to dataset created with the use of the scanning station Lecia ScanStation C10.

4.3. Registration of the ScanStation point clouds

As mentioned before, during the two days of field work, surveyors conducted full scanning of the tower. During the first day, measurement was performed using HDS targets and some features neighboring the object of interest were additionally scanned with higher quality. The-second day scanning process was conducted only using additional scanned features. These features, as well as HDS target, were required to align the point clouds into one accurate scene.

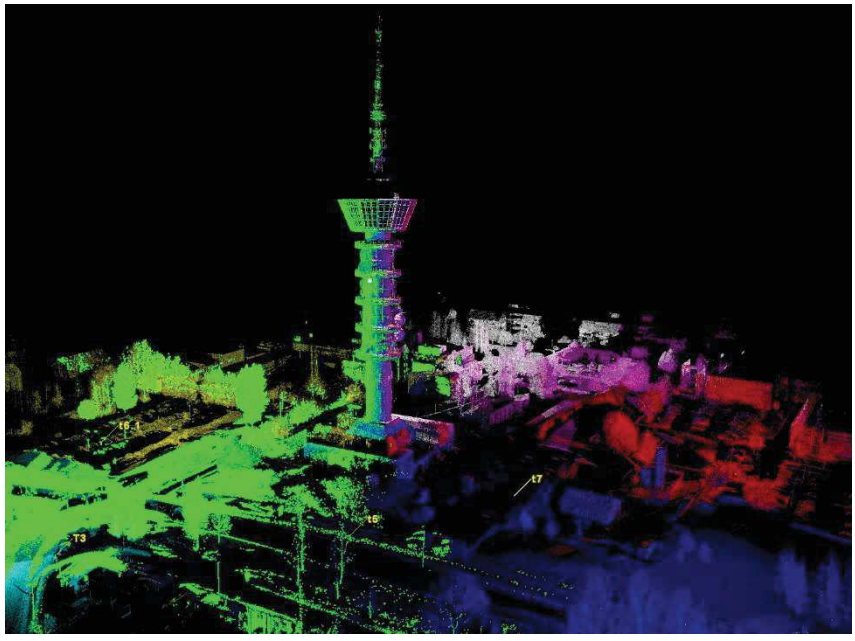

Figure 23 - Aligned scan station creating the whole scene.

The registration started in Leica Cyclone with importing point clouds of all scanning stations into the project. Two days were imported separately. In addition, particular point cloud were imported into the first-day folder. It was a text file with coordinates of the HDS targets measured at the site. The first day of measurement was registered using HDS targets but with an aid of 'cloud-to-cloud' matching process as well. The second day of measurement was combined

separately using only ‘cloud-to-cloud’ registration, with scanned with higher resolution neighboring features. After finishing both days, the final registration was performed joining them together, the important thing was to set the first-day dataset as a ‘Home ScanWorld’, due to early determination of the coordinate system in this dataset. After the final aligning the last two big point clouds following results were obtained.

The errors in the georeferenced point cloud were large for three targets, which was the reason for removing them from the final registration and adjustment.

Constraint ID	ScanWorld	ScanWorld	Type	Status	Weight	Error	Error Vector
T3	ScanWorld [Rt...	Wyniki_do_cy...	Coincident: Vertex - Vertex	On	1.0000	8 mm	(-7, 2, -3) mm
T2	ScanWorld [Rt...	Wyniki_do_cy...	Coincident: Vertex - Vertex	On	1.0000	12 mm	(11, 1, 2) mm
T4	ScanWorld [Rt...	Wyniki_do_cy...	Coincident: Vertex - Vertex	On	1.0000	13 mm	(-6, 12, -2) mm
t6.1	ScanWorld [Rt...	Wyniki_do_cy...	Coincident: Vertex - Vertex	On	1.0000	15 mm	(1, -15, 2) mm
t5	ScanWorld [Rt...	Wyniki_do_cy...	Coincident: Vertex - Vertex	Off	1.0000	29 mm	(-27, -5, 9) mm
t7	ScanWorld [Rt...	Wyniki_do_cy...	Coincident: Vertex - Vertex	Off	1.0000	40 mm	(-36, -15, -5) mm
t8	ScanWorld [Rt...	Wyniki_do_cy...	Coincident: Vertex - Vertex	Off	1.0000	40 mm	(-39, 9, -4) mm

Figure 24 - Results of point cloud adjustment on HDS targets.

Information in column ‘Status’ states for the constraint contribution in adjustment. Even after removing the three sticking out targets, the overall adjustment onto HDS targets has errors above 1 cm. This result is usually not sufficient for registration procedure, the errors should never exceed 10 mm. The reason for this might be forgetting about scanning HDS targets additionally in high resolution as separate scans.

The final cloud-to-cloud registration joining two days of field work has the error equal to 6 mm, and the error vector equal to 18 mm.

Constraint ID	ScanWorld	ScanWorld	Type	Status	Weight	Error	Error Vector
Cloud/Mes...	ScanWorld [R...	ScanWorld [R...	Cloud: Cloud/Mesh - Cloud...	On	1.0000	6 mm	aligned [18 mm]

Figure 25 - Result of final 'cloud-to-cloud' registration of two measurement days.

The Leica Cyclone is using Iterative Closest Point method for the cloud-to-cloud constraint. The user has to indicate mutual points on both point clouds, the least number of pairs is 3. To perform this algorithm, there should be a sufficient - at least 20 % - overlap of scans. It is always a good idea to scan additional, distinguish features from the surroundings. The method’s idea basically is that for each point in the first cloud, the algorithm finds the same point on the approximated surface of the second point cloud, and vice versa. Thanks to minimalizing the sum of squared distances for all of the point-to-closest surface matches, the algorithm is able to attain the optimal alignment between the two point clouds. The ultimate registration error vector is

composed of points set of the tower as well as points far apart from it for distance 30-50m, which may be the reason for rather a large alignment error.

Sometimes it happens that the ICP algorithm is not sufficiently accurate, especially for long/high objects, it is due to long scanning distances or many scan stations joined into one long project, where small errors are piling up from the beginning of registration, ending up with large errors at the end such as railway or highway projects. Thus, the HDS target aid is highly recommended for this kind of project to strengthen the constraints between scan stations.

The last step in Leica Cyclone was to export points describing the tower into a separate file, which other software may be able to support and perform further analysis. The exported dataset had roughly 9.5 million points. After removing the mast and the entrance building, dataset had 7.8 million points. The point cloud was still characterized by high density. Thus, the subsampling was performed using space subsampling method, which is taking points from the original cloud so that in output no point should be closer to another point than specified value. The specified value for this dataset was 0.015m. In the end, there are 3.8 million points creating this dataset.

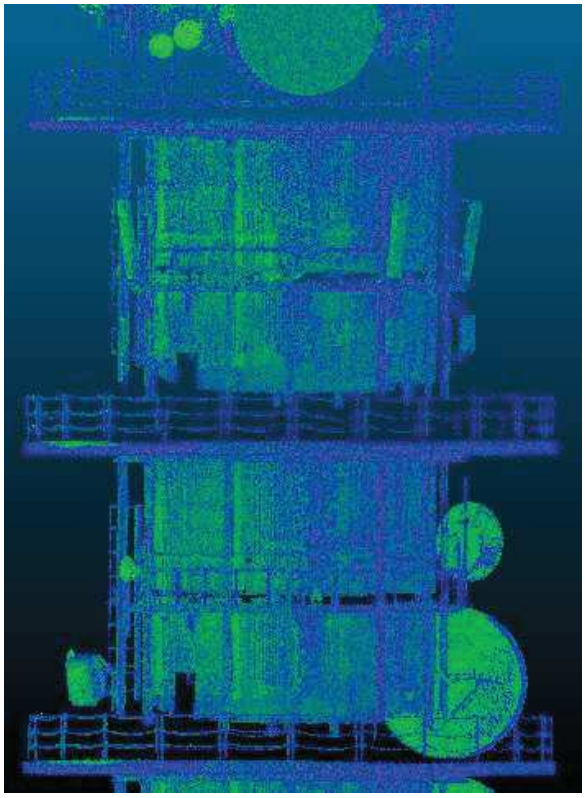

Figure 26 - Illustration of dataset gaps above the standings of the tower.

Obviously, all the scanning measurements were taken from the ground, so there are some parts where the laser could not reach, because of perspective. For example, the roof of the tower is not measured due to the perspective as well as parts right above the supportive circular standings. Fortunately for further analysis, the same problem affected angular measurement using the total station, and the selected, observed levels on the cylinder are just beneath the circular standings. The coverage of the tower is also high due to many scanning stations, there are no blank spots behind radio- or TV- transmitters.

4.4. Examination of the cylinder.

The main part of this master thesis is the comparison of obtained data. The whole comparing process is divided into two parts: the cylinder and the main gallery- presented in next

chapter 4.5. The cylinder is a high construction, about 55 meters height, and it is vulnerable on aspects like wind, solar radiation and any additional physical and chemical factors causing local or global deformation of the construction. The examination of the cylinder is performed in aspects like cross section analysis and comparison of all three methods, comparison of two dataset acquiring methods and fitting both datasets into a theoretical model of the cylinder.

4.4.1. Observed cross sections.

Examination of the cross sections is an essential aspect of this thesis, comparing results obtained using HDS and UAS measurements and theirs point clouds to the reference double-edged method, which should provide the best results thanks to its simplicity and differential calculation algorithm.

Selected datasets of cross section from both HDS and photogrammetry methods were chosen more or less on the same height as observed levels in the angular method, figure 10. The author selected 20 cm slices for each level, and for each dataset author fitted a circle.

The equation for circle is:

$$(X_i - X_c)^2 + (Y_i - Y_c)^2 = R^2$$

After writing it out, the equation has a form:

$$X_i^2 - 2X_iX_c + X_c^2 + Y_i^2 - 2Y_iY_c + Y_c^2 - R^2 = 0$$

To avoid solving quadratic equation, author introduced parameters:

$$A = -2X_c, \quad B = -2Y_c, \quad C = X_c^2 + Y_c^2 - R^2$$

The final form of the equation is:

$$AX_i + BY_i + C = -X_i^2 - Y_i^2$$

where:

X_c, Y_c – coordinates of the center of fitted circle,

R – a radius of the fitted circle,

X_i, Y_i – coordinates of the selected cross section.

The author used least squares method (LSM) to solve this problem. Datasets have over thousand points each, so the best way to determinate parameters of the circle is solving matrixes. Accuracy analysis is also calculated using matrixes.

A (i,3)				X (3,1)		L (i,1)
X_1	Y_1	1		A		$-X_1^2-Y_1^2$
X_2	Y_2	1		B		$-X_2^2-Y_2^2$
X_3	Y_3	1	x	C	=	$-X_3^2-Y_3^2$
X_4	Y_4	1				$-X_4^2-Y_4^2$
X_5	Y_5	1				$-X_5^2-Y_5^2$
X_6	Y_6	1				$-X_6^2-Y_6^2$
..	...	...				...
X_i	Y_i	1				$-X_i^2-Y_i^2$

To solve this equation, it is required to compute matrixes with the following form:

$$X = (A^T A)^{-1} \times A^T L$$

After the unknown matrix was received, the accuracy analysis was performed using, as mentioned, least squares method. The vector of residuals was calculated using formula:

$$v = AX - L$$

And covariance matrix was calculated:

$$COV(X) = \frac{\sum_1^i v_i^2}{i-3} \cdot (A^T A)^{-1}$$

Finally, the mean errors of the parameters of circle were calculated, having in mind the propagation of uncertainty parameters have following formulas:

$$mX_c = \sqrt{\frac{COV(X)_{[1,1]}}{4}}$$

$$mY_c = \sqrt{\frac{COV(X)_{[2,2]}}{4}}$$

$$mR = \sqrt{\frac{COV(X)[3,3] - 4 \cdot X_c^2 \cdot mX_c^2 - 4 \cdot Y_c^2 \cdot mY_c^2}{4 \cdot R^2}}$$

where:

$COV(X)_{[1,1]}$, $COV(X)_{[2,2]}$, ... - elements [1,1], [2,2] and so, of the covariance matrix,

X_c, Y_c, R – coordinates of the center of the circle, and its radius,

mX_c, mY_c, mR – mean errors of circle parameters.

To perform these all computation for each cross section in both acquisition methods, the author wrote a short script in MatLab. The only things to do manually were importing data and changing a number of points used for the approximation (**i**). The code, with pseudocode, is presented below.

```
%number of points taken into the approximation (only variable to
%change for each dataset
i=5621;
%translation to gain higher precision of calculations
trans = [7033000, 571000];
X = X - trans (1);
Y = Y - trans (2);

% creating matrix of factors
A = [X, Y, ones (i, 1)];

% creating vector of absolute terms
L = zeros(i,1);
for j = 1:i
    L(j)= (-1*(A(j,1))^2)-1*(A(j,2))^2;
end

% calculation the vector of unknowns' parameters
R= mtimes(inv(mtimes (A.',A)), mtimes (A.',L));
Xs= R(1,1)/(-2);
Ys= R(2,1)/(-2);

% parameters of the fitted circle
Rc = sqrt(Ys^2 + Xs^2 - R(3,1))
Xsr = Xs + trans (1)
Ysr = Ys + trans (2)

%accuracy analysis LSM
v= A*R - L;
ssq= (v.'*v)/(i-3);
COV= ssq*(inv(mtimes(A.',A)));

% mean errors of calculated parameters of the circle
mXsr =sqrt(COV(1,1)/4)
mYsr =sqrt(COV(2,2)/4)
mRc = sqrt((COV(3,3)-(4*Xs^2*mXsr^2)-(4*Ys^2*mYsr^2))/(4*(Rc^2)))
```

The translation in the imported coordinates was needed to not lose the precision of calculations. The algorithm presented above goes from very high numbers to very small, and the type double in MatLab had been not enough.

The results for the circles parameters and theirs mean errors are presented in tables below, one for laser scanning acquisition of data and second for point clouds created from photos using UAV.

Table 18 - Results of fitted circle's parameters with errors. Laser scanning data acquisition.

cross section	# points	Xc [m]	mXc [mm]	Yc [m]	mYc [mm]	R [m]	mR [mm]
1	5621	7033447.087	0.13	571477.071	0.12	3.600	0.09
2	5721	7033447.082	0.15	571477.090	0.15	3.601	0.10
3	6050	7033447.097	0.13	571477.080	0.13	3.597	0.09
4	5659	7033447.102	0.17	571477.081	0.17	3.598	0.12
5	5872	7033447.105	0.21	571477.095	0.20	3.597	0.15
6	5688	7033447.119	0.27	571477.124	0.26	3.597	0.19
7	5224	7033447.115	0.32	571477.145	0.30	3.597	0.21
8	5242	7033447.106	0.33	571477.157	0.32	3.597	0.22

Table 19 - Results of fitted circle's parameters with errors. UAV data acquisition.

cross section	# points	Xc [m]	mXc [mm]	Yc [m]	mYc [mm]	R [m]	mR [mm]
1	1318	7033447.092	0.86	571477.041	0.88	3.607	0.67
2	1611	7033447.081	0.42	571477.050	0.43	3.602	0.35
3	1508	7033447.089	0.77	571477.049	0.79	3.608	0.67
4	1494	7033447.092	1.30	571477.032	1.38	3.619	1.32
5	1279	7033447.098	1.46	571477.060	1.50	3.606	1.26
6	1768	7033447.097	0.66	571477.084	0.66	3.602	0.61
7	1398	7033447.075	1.54	571477.110	1.39	3.606	0.88
8	2537	7033447.079	0.56	571477.119	0.59	3.608	0.51

The difference in quantity between two data acquisition approaches is almost 4-folded, remembering about the subsampling from 7.8 million to 3.8. This disproportion may have a small impact on the mean errors of calculated circles' parameters. The mean errors are much larger for point cloud made out of pictures from the drone.

Analyzing the point cloud made out of laser scanning measurements, it is possible to notice that coordinates of the centers of the fitted circles present tendency to leaning back the tower into the north-east direction. The mean errors of centers' coordinates have expected trend of increasing.

It is due to the length of the laser beam for each higher cross section was increasing and the measurement might have been less accurate, the only one exception is noticed for second observed level, where both errors are slightly higher than the errors of the level above.

The only known value of the tower is its diameter, thanks to Norwegian article in Wikipedia, and should be equal to 7.2 meters. So the radiuses of fitted circles should be equal to 3.6m, the results show very small differences from the known radius value. As it was expected, the radiuses differ one from another, but here it is also possible to see the following trend of the size of it. The higher cross section was the bigger difference from the known value. In addition, the radiuses' mean errors are also larger when the cross section was located higher. All these observations conform to expectations of laser scanning measurements. The higher point was measured, the longer laser beam was and more acute angle of incidence, these factors led to lower quality of computed point, which resulted in higher and higher mean errors for circle's parameters for higher cross sections.

The selected cross section from the point cloud obtained from pictures using UAV do not show any tendency in evaluated results. The center's coordinates do not differ from each other, but the differences are alternately changing. They do not follow the same inclination's trend as in the case of the angular method and laser scanning. All estimated radiuses from these datasets differ from the known value. The biggest deviation is observed at fourth level, almost 2 cm. The results do not show any tendency actually. The mean errors of the circles' parameters also vary independently from the height of cross section. This method does not provide any insight for a location of accuracy on the computed dataset. Comparing mean errors of both methods of data acquisition, there is a great disproportion between them, partially due to the number of points representing a cross section, partially due to not removed noises from photogrammetry created point cloud, but mainly the poor quality of point cloud computed overall.

To calculate the components of the inclinations, coordinates of center of the circles were used and given formula:

$$w_X^j = X^j - X^1$$

$$w_Y^j = Y^j - Y^1$$

where:

X^j, Y^j, X^1, Y^1, - accordingly coordinates of the geometric center of j-th and the most bottom cross section, j=1, 2…, 8.

Author listed component inclination of the tower from all three methods, and the table below presents the results.

Table 20 - Comparison of component inclinations from all three methods.

		L1	L2	L3	L4	L5	L6	L7	L8
double -edged method	wx [mm]	0.0	-4.9	9.2	14.1	18.9	24.5	32.6	15.9
	wy [mm]	0.0	15.5	1.7	2.5	10.4	33.8	59.1	71.8
laser scanning	wx [mm]	0.0	-4.6	10.4	15.6	18.8	31.8	27.8	19.2
	wy [mm]	0.0	18.7	8.4	10.2	23.9	52.3	73.3	85.5
UAV	wx [mm]	0.0	-11.3	-3.6	-0.8	5.9	4.7	-17.7	-13.6
	wy [mm]	0.0	9.0	7.7	-9.6	18.3	42.4	68.9	77.8

As mentioned previously, the inclination computed from UAV method is not characterized by any trend. The comparison shows that laser scanning actually follows the results of the double-edged method. For inclination on X-axis they match close to themselves, on Y-axis, they drift away a little bit. The reason for that may be few HDS targets near the object were set and measured. Three of them were actually excluded from registration process due to higher error vertexes, and the registration 'cloud-to-cloud' may be not satisfying for higher parts of the tower. Therefore, at this point, we may conclude that the photogrammetry applications for inventory of the high construction using the camera mounted on the DJI Phantom 3 Professional. The further analysis concerns the main gallery located at the top of the cylinder.

4.4.2. Comparison of two data acquisitions methods.

Additional 'cloud-to-cloud' alignment was performed, only for the cylinder in both data acquisition methods, all elements on the tower, as well as the main gallery, were removed from both point clouds. In CloudCompare software the alignment was performed at first. It was needed due to the differences in centers of the circles' coordinates. The mean difference at north-coordinates is 3.8 cm and at east-coordinates the difference equals to 1.5 cm. Thereafter, distance computation was carried out.

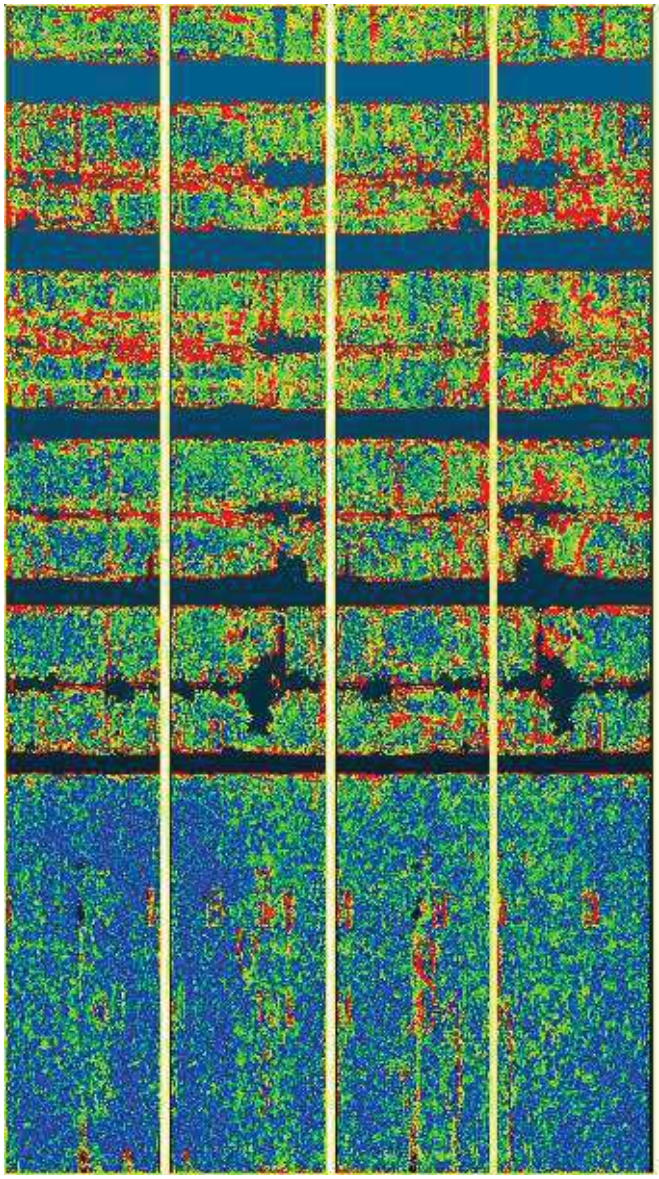

Figure 27 - 4 sides of the cylinder (without any elements on it). From left to right accordingly: south, east, north and west side.

The figure next to presents the distances between two point clouds. The red color starts for spans longer than 3 centimeters. It is easy to notice that these values are usually agglomerated near areas of the removed or not measured points, for example, areas where the laser scanning method could not reach the surface of the cylinder it is noticeable slim-line of the red points. The most of red color pixels are located in the top prat of the cylinder, it is because of many elements removed from there. In figure 28 is presented the histogram of computed distances from UAV point cloud to the locally modeled reference mesh obtained from laser scanning. The range of distances was set from 0.0 to 7.0 cm, any larger spans were qualified as lack of points on the reference cloud. In total, the histogram has roughly 451 thousands of sampled points. 35% of points do not exceed 0.5 cm distances, 61% of them are shorter than 1.0 cm, about 75% has 1.5 cm limitation, and almost 84% of them do not surpass 2.0 cm distances.

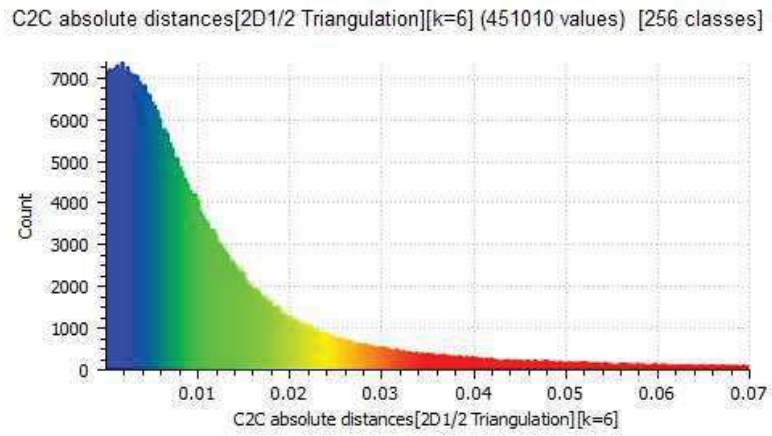

Figure 28 - Histogram of computed distances from point cloud to reference locally modeled mesh.

The important thing to know about the distance computation in CloudCompare is that if the datasets are with the similar amount of points and none settings changed the distance will be calculated to the nearest neighboring point of the reference point cloud. Whereas the reference point cloud is denser than the modeling one, it is strongly advised to change setting in 'Local modeling' for '2D ½ Triangulation'. This treatment will cause a local modeling, from reference point cloud into a mesh. Then the cloud to mesh distances are computed. 'This [operation] is statistically more precise and less dependent on the cloud sampling (it can locally produce *strange* results - as the modeling phase is very limited - but it gives much better results on a global scale)'[1].

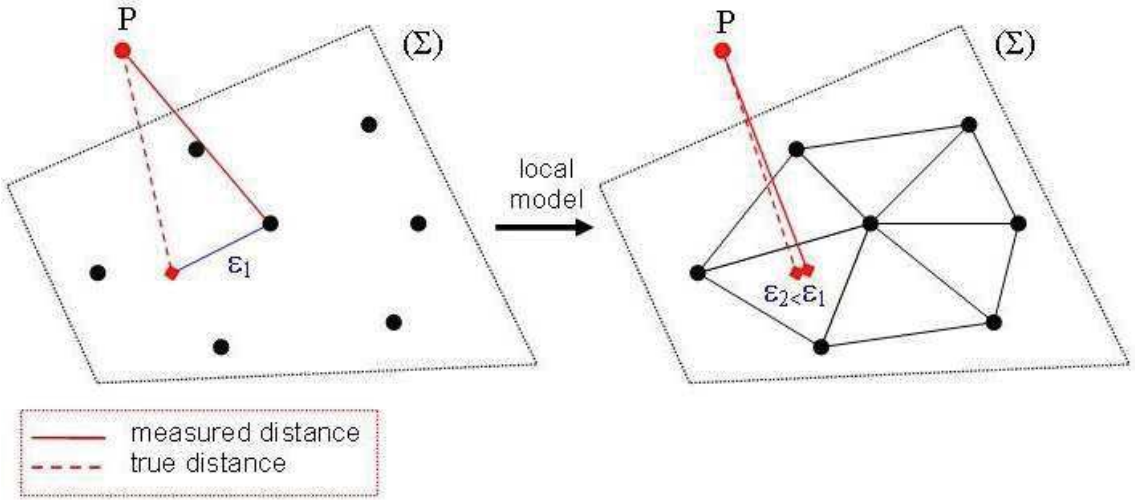

Figure 29 - Difference in error in distance computed to the nearest neighboring point and using local modeling. [1]

In conclusion the distances computed using local modeling are characterized by smaller errors, the best scenario would be to obtain the global model of the surface, it would more accurate and simpler to compute distances from the compared point cloud to model.

4.4.3. Alignment of point clouds into created theoretical model.

The theoretical model was created in the CloudCompare using 'Primitive Factory' tool. The known dimensions of the cylinder are the height and the radius, accordingly 55.6m and 3.6m. The translation of the cylinder was performed manually, roughly aligning the model to the point cloud in both cases of data acquisition methods. The important thing to remember was to increase the precision of modeled cylinder, due to generalization the model might have had 24 lateral faces, but the author increased it to 80- faces on the lateral surface, as the reference model, significantly decreasing approximation error. The cloud to mesh distances were calculated for both data acquisition methods. Histograms of these computations are presented in figure 30 and 31.

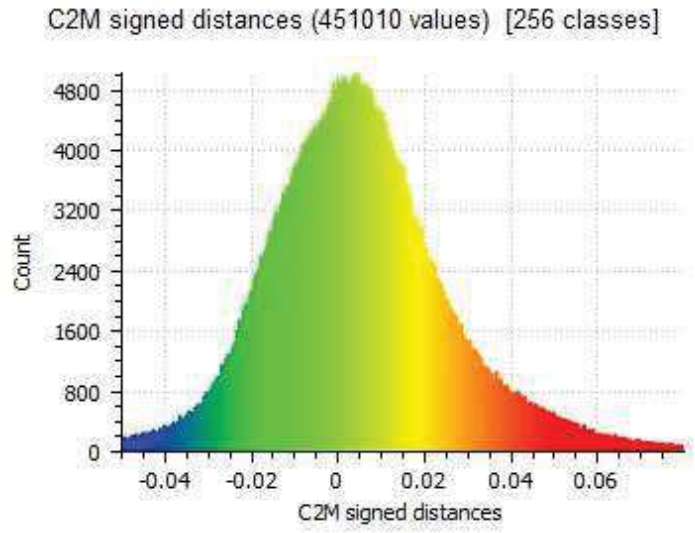

Figure 31 - Histogram of computed signed distances from UAV's point cloud to the model.

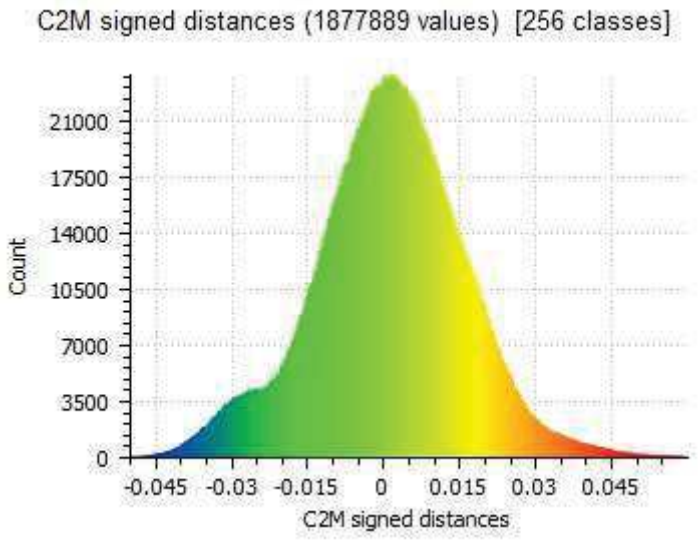

Figure 30 - Histogram of computed signed distances from laser scanning's point cloud to the model.

Both graphs present good examples of Gaussian curve. Whereas the difference in sampled data set is 4 times higher for laser scanning data acquisition method, which might be the reason for a smoother looking graph.

To have better insight in how the computed distances are located on the object author compared both point clouds from the west and east side as an example. Of course for both comparisons the blue color represents 'negative' distances (points 'inside' the modeled cylinder) longer than 5 cm, and red color represented 'positive' distances also longer or equal to 5 cm.

It is easy to notice the same location for orange and red agglomerations but is it also noticeable that in the case of 3D point cloud made out of pictures using UAV these agglomerations are more spread, which implies that the quality of dataset is worse. In the case of laser scanning point cloud the transitions between colors are smoother and long distances are represented by the fewer group of points. On the right side, the depicted east side of the tower, the figure shows the longer distances in the upper part, it indicates to leaning back the tower toward the east direction, as it was computed in chapter 4.4.1. This overall visualization might be useful for examination of the whole tower and looking for small changes in the tower's coat. Manipulation of displayed distances and saturation may be useful to even better understand the dataset, and estimate the quality of the object. This approach may be used for laser scanning method which has more predictable patterns of error propagation. In the case of point cloud made out of pictures captured from the drone, the single errors occur more often. To obtain better quality point cloud, surveyors should have used a better camera on the drone. And increase the expertise of point cloud densification process in software Pix4D mapper.

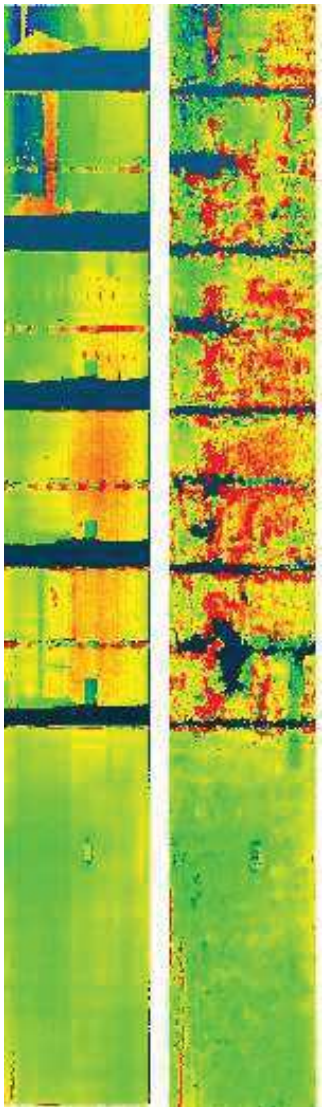

Figure 32 - Comparison of calculated signed distances for both data acquisition approaches, presenting the west side of the tower.

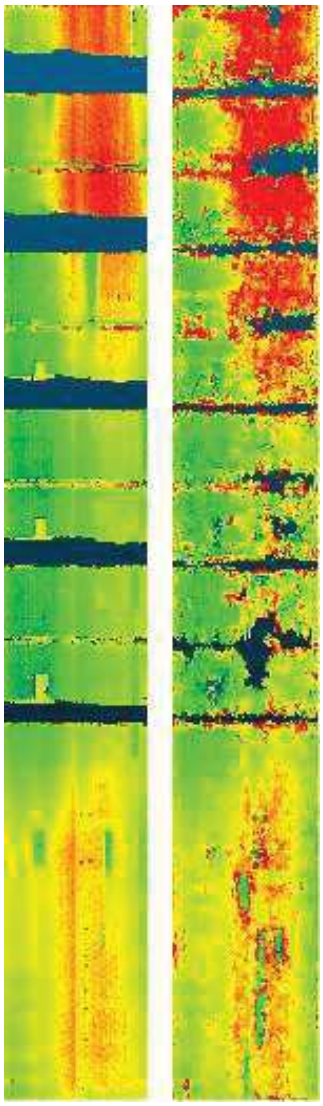

Figure 33 - Comparison of calculated signed distances for both data acquisition approaches, presenting the east side of the tower.

4.5. Analysis of the main gallery.

The last part of data analysis is the examination of the main gallery, for this particular construction author does not have any information about the sizes of any elements creating this object. Thus, the determination of the quality of attained datasets will be evaluated based on them

itself, comparing coordinates of measured points at the prism with totals station and one obtained from clouds, and fitting one point cloud into another.

4.5.1. Coordinates' comparison.

These mentioned coordinates were obtained during the first day of measurement using the total station and survey reflectorless distances to the vertexes of the main gallery. These points were used in software Pix4D mapper as geographical reference for computing the densified 3D point cloud from taken pictures.

Table 21 - Coordinates of GCPs located at the main gallery.

ID	Y [m]	X [m]	Z [m]
GD1	571473.846	7033439.995	180.091
GD2	571470.762	7033442.598	180.091
GD3	571469.402	7033446.397	180.083
GD4	571470.075	7033450.354	180.092
GD10	571484.168	7033443.785	180.075
GD11	571481.597	7033440.720	180.094
GD12	571477.807	7033439.315	180.108
GG1	571472.358	7033436.834	188.589
GG2	571467.870	7033440.581	188.551
GG3	571465.868	7033446.112	188.552
GG4	571466.890	7033451.863	188.541
GG11	571483.608	7033437.762	188.546
GG12	571478.125	7033435.799	188.584
GD5	571472.699	7033453.418	180.138
GD6	571476.448	7033454.791	180.128
GG5	571470.662	7033456.337	188.611
GD9	571484.905	7033447.744	180.073
GD8	571483.513	7033451.534	180.060
GG8	571486.438	7033453.505	188.511
GG9	571488.441	7033448.018	188.513

Figure 34 - Visualization of the scheme of a naming of GPCs. GG stands for the upper edge of the tower, GD for the bottom edge of the tower, and numbering of edges starts with the most south one and increasing clockwise.

The drone's point cloud should have an advantage, since these points were used for georeferencing the result 3D point cloud. However, all measurements were based on the same adjusted network, so there should be convergence in calculated distances and their accuracy obtained from laser scanning method because of the HDS targets were tied to the established network.

Calculation for the dataset obtained from the UAV, we automatically made in the software Pix4d mapper during the 'Initial Processing'. Results of the errors in 3 different axes were given

in the report (Appendix 4 - 'Pix4D mapper – final point cloud's report'). Author erased five points which were not located in the main gallery and recalculated the mean value and the standard deviation.

Table 22 - Error's components from Pix4d mapper final report.

GCP Name	Error X [m]	Error Y [m]	Error Z [m]
GD1	0.019	0.005	-0.010
GD2	0.008	-0.001	-0.003
GD3	0.014	0.015	-0.003
GD4	-0.009	0.001	-0.007
GD10	-0.014	0.003	-0.008
GD11	0.005	0.033	-0.011
GD12	0.010	0.012	-0.004
GG1	-0.001	0.009	0.007
GG2	-0.007	-0.013	0.000
GG3	-0.001	0.001	0.004
GG4	-0.038	-0.023	-0.018
GG11	-0.032	-0.028	-0.005
GG12	-0.006	0.006	-0.002
GD5	-0.012	0.011	0.012
GD6	-0.033	0.022	-0.003
GG5	-0.006	0.002	0.023
GD9	0.004	-0.007	-0.003
GD8	-0.009	0.000	-0.004
GG8	0.038	-0.008	-0.009
GG9	0.031	-0.001	0.001
GG10	0.020	0.000	0.002

The calculated mean and standard deviation values are for:

- X-axis: -0.0009 ± 0.0192 m,
- Y-axis: 0.0019 ± 0.0134 m,
- Z-axis: -0.0020 ± 0.0084 m.

Obviously, the mean values are very low, due to the fact that the point cloud has been fitted into that control points located at the vertexes of the main gallery. However obtained standard deviations are rather large, due to residuals for some points or theirs components, for example, points GD11, GG4, GD6, GG8, and GG9. These residuals may have the origin from not precise pointing at measured vertex of the main gallery, as well as the influences of the length, steep

vertical angle and material of the surface. The standard deviation of the errors' components (describing error of the distance) equals to ±0.025 meter.

From the laser scanning point cloud, the author selected points which describe the vertexes measured with the total station. The comparison of them may be found in table 23.

Table 23 - List of vertexes' coordinates from the total station and from the laser scanning dataset.

	Coordinates from total station			*Coordinates picked from laser scanning point cloud*		
ID	*Y [m]*	*X [m]*	*Z [m]*	*Y [m]*	*X [m]*	*Z [m]*
GD1	*571473.846*	*7033439.995*	*180.091*	*571473.867*	*7033440.018*	*180.107*
GD2	*571470.762*	*7033442.598*	*180.091*	*571470.815*	*7033442.616*	*180.094*
GD3	*571469.402*	*7033446.397*	*180.083*	*571469.433*	*7033446.376*	*180.101*
GD4	*571470.075*	*7033450.354*	*180.092*	*571470.110*	*7033450.376*	*180.093*
GD10	*571484.168*	*7033443.785*	*180.075*	*571484.214*	*7033443.829*	*180.090*
GD11	*571481.597*	*7033440.720*	*180.094*	*571481.580*	*7033440.718*	*180.108*
GD12	*571477.807*	*7033439.315*	*180.108*	*571477.854*	*7033439.346*	*180.127*
GG1	*571472.358*	*7033436.834*	*188.589*	*571472.399*	*7033436.863*	*188.591*
GG2	*571467.870*	*7033440.581*	*188.551*	*571467.920*	*7033440.596*	*188.553*
GG3	*571465.868*	*7033446.112*	*188.552*	*571465.898*	*7033446.119*	*188.557*
GG4	*571466.890*	*7033451.863*	*188.541*	*571466.912*	*7033451.881*	*188.577*
GG11	*571483.608*	*7033437.762*	*188.546*	*571483.680*	*7033437.840*	*188.570*
GG12	*571478.125*	*7033435.799*	*188.584*	*571478.159*	*7033435.890*	*188.477*
GD5	*571472.699*	*7033453.418*	*180.138*	*571472.711*	*7033453.433*	*180.123*
GD6	*571476.448*	*7033454.791*	*180.128*	*571476.498*	*7033454.823*	*180.107*
GG5	*571470.662*	*7033456.337*	*188.611*	*571470.687*	*7033456.362*	*188.587*
GD9	*571484.905*	*7033447.744*	*180.073*	*571484.917*	*7033447.732*	*180.099*
GD8	*571483.513*	*7033451.534*	*180.060*	*571483.548*	*7033451.552*	*180.086*
GG8	*571486.438*	*7033453.505*	*188.511*	*571486.421*	*7033453.566*	*188.535*
GG9	*571488.441*	*7033448.018*	*188.513*	*571488.434*	*7033448.077*	*188.539*

The differences between coordinates were calculated, as well as the mean values and standard deviation for 3 dimensions, and the overall mean and standard deviation describing the spatial distance.

Table 24 - Differences between coordinates.

ID	*dX [m]*	*dY [m]*	*dZ [m]*
GD1	*-0.021*	*-0.023*	*-0.016*
GD2	*-0.053*	*-0.018*	*-0.003*
GD3	*-0.031*	*0.021*	*-0.018*
GD4	*-0.035*	*-0.022*	*-0.001*
GD10	*-0.046*	*-0.044*	*-0.015*

GD11	*0.017*	*0.002*	*-0.014*
GD12	*-0.047*	*-0.031*	*-0.019*
GG1	*-0.041*	*-0.029*	*-0.002*
GG2	*-0.050*	*-0.015*	*-0.002*
GG3	*-0.030*	*-0.007*	*-0.005*
GG4	*-0.022*	*-0.018*	*-0.036*
GG11	*-0.072*	*-0.078*	*-0.024*
GG12	*-0.034*	*-0.091*	*0.107*
GD5	*-0.012*	*-0.015*	*0.015*
GD6	*-0.050*	*-0.032*	*0.021*
GG5	*-0.025*	*-0.025*	*0.024*
GD9	*-0.012*	*0.012*	*-0.026*
GD8	*-0.035*	*-0.018*	*-0.026*
GG8	*0.017*	*-0.061*	*-0.024*
GG9	*0.007*	*-0.059*	*-0.026*

The calculated mean and standard deviation values are for:

- X-axis: -0.0287 ± 0.0228 m,
- Y-axis: -0.0275 ± 0.0272 m,
- Z-axis: -0.0044 ± 0.0301 m.

In that case, the mean values are noticeably larger than in previous calculations, as it was expected the point cloud made of the pictures had smaller values due to the global alignment on them. Whereas, the mean values for the laser scanning show that the coordinates are shifted north and west directions. It might be connected with the inclination of the tower, but more likely it is related to the registration process of the scan stations.

From visual observation of the gallery dataset and measured vertexes of it, most of the GCPs were outside the model. It indicates of small shrinkage of the 3D point cloud, it also follows the trend from the cylinder's analysis. There was a tendency to shrinking the radius of the observed cross sections the higher there were located. Part of main gallery's shrinkage is a cause by the previous one appeared at the cylinder.

4.5.2. 'Cloud-to-cloud' comparison

The examination of this part is determined without the roof, due to the perspective from obtaining laser scanning dataset method, it is only viable manner for this comparison. The roof was removed from the point cloud in drone's data acquisition approach, and the ladder attach to the main gallery accessing the roof was removed also from both datasets.

The main visual observation on the both dataset is that the one obtained from laser scanning. It has no points at the windows, the laser beam reflected only from the metal parts of the gallery. The drone's point cloud has small groups of the point at the windows in the corners of them.

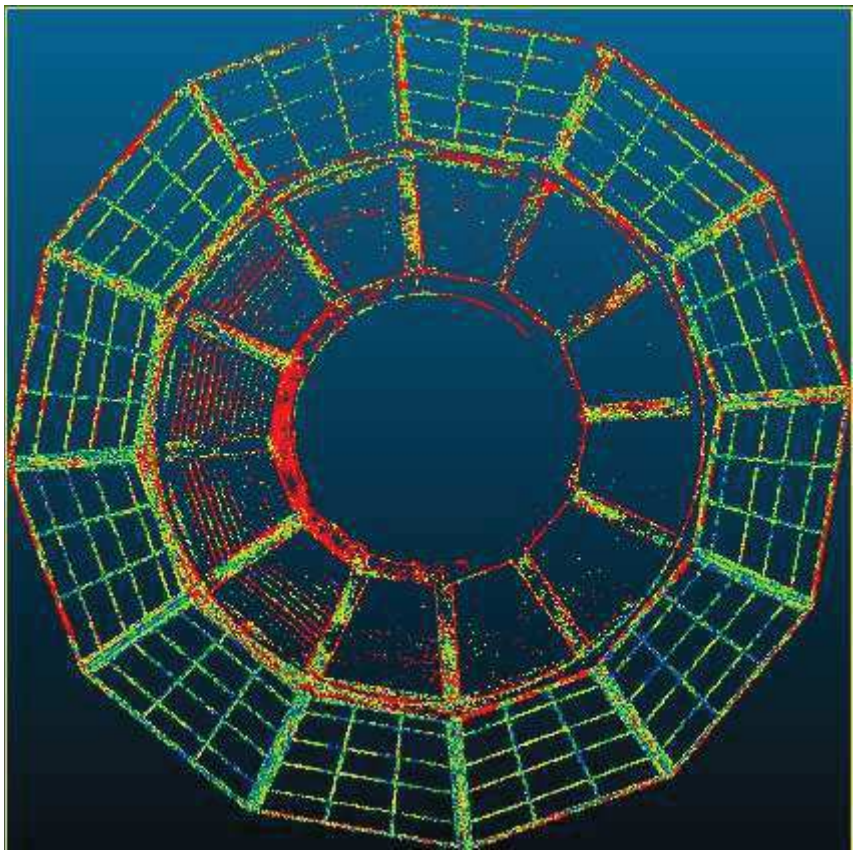

Figure 35 - Top view of the main gallery. Cloud to cloud spatial distances.

Reference: drone point cloud. Model: laser scanning point cloud.

The figure above presents the computed distances between two datasets of the main gallery. The reference data is one obtained from UAV, and model from laser scanning. The blue color pixels indicate distances shorter than 1 cm, and the red color is in a range from 4 to 8 cm, every pixel with larger than 8cm distance is not shown in this figure. The reason for picking the drone's point cloud as the reference is the fact that in the previous subchapter, author shown the advantage of drone's cloud, due to the georeference into points onto the tower. The second reason for choosing the drone's dataset is a higher number of points describing the main gallery. The distance calculation was performed using (as in the case of the cylinder) local modeling setting available in the CloudCompare program, choosing '2D ½ Triangulation' (see figure 29 for explanation).

The lateral surfaces of the main gallery are made out of steel frames and their differences in position (comparing both point clouds) seems to have the connection with the more and less

lighting side of the gallery. At the bottom of the figure is the south part of the object, this part is characterized by a higher number of blue points representing small values of the distances. Whereas the top of the image depicts the north, less-lit side, of the object having higher number of green-yellow-red points.

In addition, the figures from 36 to 38 show distances from cloud to cloud in 3 separated directions. Accordingly, distances along X-axis, Y-axis, and Z-axis.

CloudCompare software works on the mathematical coordinate system. Thus, the X-axis is going from left to right (on all figures, from 36 to 38) and Y-axis goes from bottom to top.

In all three figures, the blue color describes values from -5.0 to -3.0 cm, coming through green where values are equal to 0.0 cm and going into orange and red for values from 3.0 cm to 5.0 cm.

As in the case of the spatial distances, here it is also noticeable that longer spans are in the north, less-lit area of examinations. In every case of on split X, Y and Z components the green color is always in the middle of the element, usually surrounded by a bit darker green and yellow. The reason for it is that the computation is made to the referenced locally modeled point cloud from drone, and the middle parts have always the closest way to it or are on the modelled cloud already.

The author examined histograms of these three computations and calculated the percentage of points within certain limits.

X compartment of point cloud (roughly 245 thousands points): from -0.03 to 0.03 m: 89.0%, from -0.02 to 0.02 m: 72.9%, from -0.01 to 0.01 m: 41.8%.

Y compartment of point cloud (about 244 thousands points): from -0.03 to 0.03 m: 90.5%, from -0.02 to 0.02 m: 75.0%, from -0.01 to 0.01 m: 43.0%.

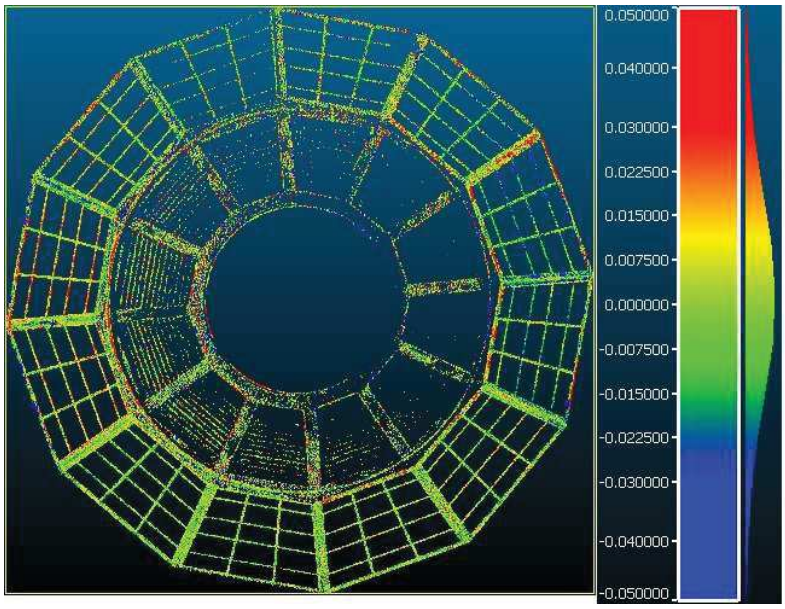

Figure 36 - Residuals along X-axis. Reference: drone point cloud. Model: laser scanning point cloud.

Z compartment of point cloud (236 thousands points): from -0.03 to 0.03 m: 90.9%, from -0.02 to 0.02 m: 76.0%, from -0.01 to 0.01 m: 42.9%.

These boundaries were chosen to illustrate the distribution of a value of the point in areas between blue and red color. Starting from 1 cm limit as an error of the measurement and increasing it by a particular standard deviation. Unfortunately, the values are dissatisfying, less than half of points do not meet the requirement of spans shorter than 1 centimeter. The reason for that might be mentioned shrinkage of the laser scanning point cloud due to the length of the laser beams reaching the highly located gallery and partly errors made in the registration process.

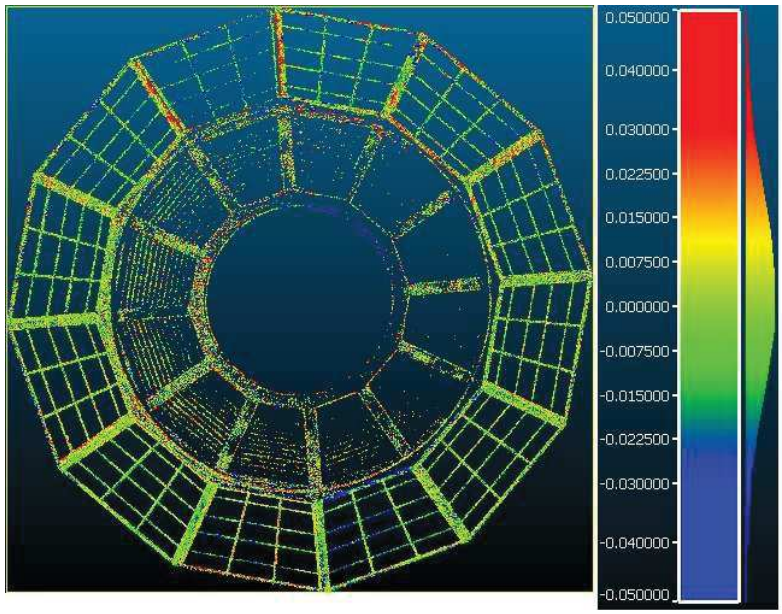

Figure 38 - Residuals along Y-axis. Reference: drone point cloud. Model: laser scanning point cloud.

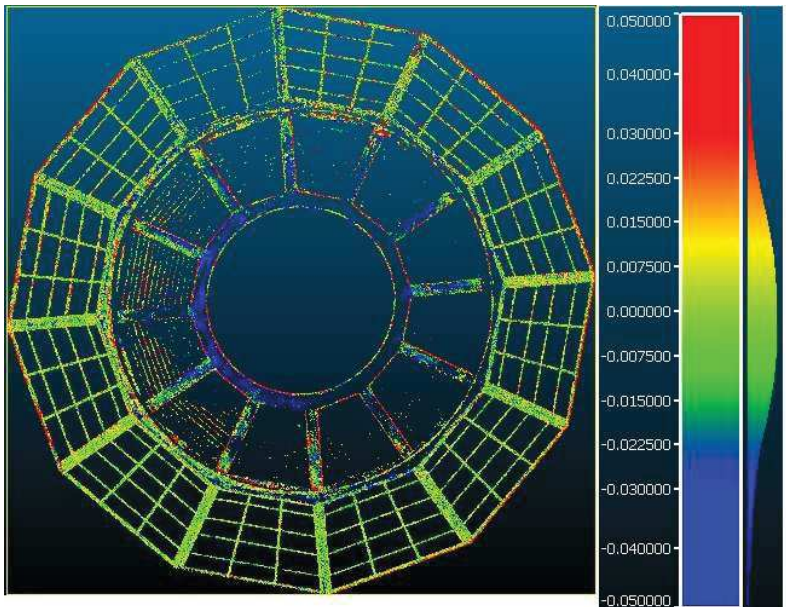

Figure 37 - Residuals along Z-axis. Reference: drone point cloud. Model: laser scanning point cloud.

In brief conclusion, the dataset obtained from a drone is better than one attained from a laser scanner. The reason for that may be a large number of GCPs on the main gallery, which resulted in better georeferenced and better manner in keeping correct dimensions. Unfortunately, the author has not information about any sizes of the main gallery. So the comparison is impossible in this aspect.

5. Conclusion

The selected land surveying methods for this particular task performed very well. The reference component inclinations obtained from double-edged method are based on only angular measurements, and very advanced and higher resource-required method - the High Definition

Surveying using scan station - is based on fast measuring distances and angles, and calculating the position of every point measured. The author is going to bring his thoughts upon post-processing and suggestions of improvement closer to the readers.

5.1. Thoughts on post-processing

Results from the double-edged method were treated as unflawed, but the standard deviation for two out of eight levels was characterized by larger values than the others. The first assumption was a deviation from circularity of the cylinder's cross sections. However, in the further process, the fitted circles into selected data sets of observed levels did not show the same tendency. The reason for that is probably not precise aiming at the edge of the cylinder because of many elements mounted at the surface of the tower.

The whole post-processing gives a rather good insight what are the possibilities of this specified drone. The Author had to learn more about deliverables which provides the software Pix4D mapper and theirs quality. From this process, we may conclude that the taken pictures had a huge scope, there were surroundings which were not a part of the object of interest that also produced vast noises around the tower in many cases during 3D point cloud densification. The important issue in capturing photos was lighting, it comes obvious that better-lit side of the tower was presented denser and with a better quality point cloud. The certain thing is the more pictures the better, even when author picked only half of photos, in one case the 3D point cloud was representing the whole object but with quite a few points. The quantity of pictures increase the time needed for the software to process all the data but for high-tech computers would not cause any big problems.

Registration of point clouds obtain from scan station measurements was performed in Leica Cyclone software. As it was mentioned, the author used registration on the HDS targets aided with 'cloud-to-cloud' registration on additionally scanned features around the object for the first day of measurement, and there was used only 'cloud-to-cloud' method for data obtained the second day. It resulted in not very good alignment of stitched scan station presented in chapter 4.3. It might have been caused by few HDS points set during the field work, as well as the 'cloud-to-cloud' is not as good for tall constructions, and it is lacking tie points in the upper part of it.

Comparison of two datasets: UAV and laser scanner in terms of visual content show that the laser scanning has a great advantage over point cloud from photogrammetry method. The coverage and density are better, the only parts not covered by laser scanning are right above the

standing and main gallery, where due to perspective ground scan station did not reach the surface, these ones are covered by UAV's point cloud.

Point clouds depicting cylinder were compared in terms of inclination of the tower. The coordinates of the centers and radiuses were calculated. The results from laser scanning method were very much alike with the reference method. However the results from drone's point cloud were not satisfying, the values did not match nearly at any observed level. Comparing 3D point clouds with the theoretical model of tower's cylinder gave, at first sight, similar results, but for the cloud from photogrammetry method higher percentage of points were characterized by larger residuals from the model. This process also allowed to visually check the inclination of the cylinder.

For main gallery 3D point clouds, there was conducted the examination of the datasets their selves, due to lack of information about projected sizes and dimensions of particular elements of the main gallery. In this case, the point cloud showed up as better. The cloud's density was higher and had information about the roof of the main gallery, laser scanning could not reach that part because of the perspective. This result might have been achieved for many points measured at the vertexes of the main gallery and the photogrammetry point cloud was fitted into it, preserving adequate scale and position.

In general, the author thinks that the laser scanning method performed better at the cylinder part of the examination, but the UAV's dataset had many assets while studying the main gallery. In photogrammetry method 21 so-called ground control points were measured at the main gallery which was the probable cause of better results in this part rather than the cylinder, whereas the cylinder had 5 of them. Both methods of data acquisition complement each other drawbacks in this particular project. Author has received the feedback from a person who did many 3D models, and he commented this project as very difficult, most of the tower he modeled from the terrestrial laser scanning, but elements not shown in this dataset were replaced by the photogrammetry 3D point cloud and sometimes pictures taken with the UAV.

5.2. Suggestions for improvements

The whole process does not give the explicit answer for the hypothesis formulated at the beginning of the thesis. Part of the object were displayed better in terrestrial laser scanning, and other parts in UAV's point cloud had better quality. The author came out with some suggestions for improving the similar project in the future, but he had no time to do it individually.

The obvious thing to change is the UAV and its sensor. The camera mounted on the unit may have been too small, and to achieve better, smaller ground sampling distance and in result have higher spatial resolution with more visible details. The alternative for this improvement would be even more photos with a shorter distance to the tower. That would also increase the visibility of details and spatial resolution of deliverables. The shorter distance from camera to the object could increase the possibility to crash UAV into some protruding elements during unit was doing the circle around. A different approach would be needed to avoid unpleasant and dangerous collision of the drone, for example making photos in columns that would reduce the risk and solve the problem with uneven ground sampling distances in different parts of the object, as the spans between the unit and the object were unequal.

The field work was performed in winter's month, both measuring days were with very similar atmospheric conditions to eliminate external factors changing the geometry of the tower. However, this period of time is not the best for any field work requiring lighting. The days were short, and the sun was quite low above the horizon, that could be the reason for worse exposure of the pictures taken from the north side of the tower. The late spring's or early summer's months would be probably the best because the sun is higher above the horizon, this is also the best period of time to do any photogrammetric projects due to weather conditions.

Laser scanning process done during the field work was conducted on too few HDS targets, they should have been distributed around the object. 3 targets out of 7 were removed from the final alignment due to very large error vectors on them, the solution to avoid this problem or minimize is to additionally scan all targets on a very high resolution, and this will help the software to better estimate the center of each HDS target.

The examined building could have been taller. That would give better insight at what height the unmanned aerial photogrammetry is better than terrestrial laser scanning. Surveyor would have to cover the object with many, evenly distributed and identifiable points on the whole surface of examined construction. These points would help the unmanned aerial photogrammetry to obtain better and more accurate deliverables.

The most ideal situation would be mounting the laser scanner at the unmanned aerial vehicle, these solutions have been implemented by some companies around the world.

References

[1] CloudCompare manual - http://www.danielgm.net/cc/doc/qCC/Documentation_CloudCompare_version_2_1_eng.pdf [Accessed 10.06.2016]

[2] Dz.U. 2013 poz.1032 – Polish regulation about classification of aerial vehicles.

[3] J. Bernasik, "Realia i Perspektywy Pomiarów Odkształceń", 2001

[4] I. Colomina, P. Molina, "Unmanned aerial systems for photogrammetry and remote sensing: A review", 2014 https://www.researchgate.net/publication/261290207 [Accessed 12.06.2016]

[5] H. Eisenbeiss, "UAV Photogrammetry", 2009, pp.1-20, 44-53, 143-167.

[6] A. Fryśkowska, M. Kędzierski, "Chosen Aspects of Terrestrial and Aerial Laser Scanning Data Integration", 2010

[7] R. Gawałkiewicz, „The Inventory of High Objects Applying Laser Scanning, Focus on the Cataloguing a Reinforced Concrete Industrial Chimney", 2015

[8] J. Gocał, "Geodezja inżynieryjno- przemysłowa –cz. III", 2003, pp. 329-375.

[9] M. Kędzierski, A. Fryśkowska, D. Wierzbicki, „Opracowania fotogrametryczne z niskiego pułapu", 2014

[10] R. Kocierz, "Ocena oddziaływania wpływów termicznych na wyniki geodezyjnych pomiarów przemieszczeń budowli żelbetowych" - doctoral thesis, 2014.

[11] J. Królikowski, "Na drony przyjdzie jeszcze czas" an interview, 2015, https://geoforum.pl/?menu=47064,47149,47150 [Accessed 10.06.2016]

[12] G. Lenda, „Badanie zasięgu i dokładności dalmierzy bezzwierciadlanych", 2003

[13] G. Lenda, U. Marmol, „Dokładność dalmierzy bezzwierciadlanych dla pomiaru obiektów wykonanych z materiałów syntetycznych", 2010

[14] F. J. Mesas-Carrascosa, I. C. Rumbao, J. A. Barrera Berrocal, A. Garcia-Ferrer Porras, "Positional Quality Assessment of Orthophotos Obtained from Sensors Onboard Multi-Rotor UAV Platforms", 2014, www.mdpi.com/journal/sensors [Accessed 12.06.2016]

[15] B. Mitka, Ł. Mikołajczyk, T. Noszczyk, „Modelling of Industrial Facilities Based On Data from Terrestrial Laser Scanning", 2013

[16] S. Sabbatini, „Pros and cons of 3D laser scanner vs. traditional techniques", 2015, http://www.3dscan.it/en/blog/pros-and-cons-of-technology-3d-laser-scanner-than-traditional-survey-techniques/ [Accessed 10.06.2016]

[17] D. Turner, A. Lucieer, S. M. de Jong, "Time Series Analysis of Landslide Dynamics Using and Unmanned Aerial Vehicle (UAV)", 2015, www.mdpi.com/journal/remotesensing [Accessed 12.06.2016]

[18] A. Wróbel, A. Wróbel, „Termografia w pomiarach inwentaryzacyjnych kominów przemysłowych – cz. II", 2012 www.inzynierbudownictwa.pl [Accessed 10.06.2016]

[19] M. Żak, "Geodezyjna obsługa wznoszenia komina żelbetowego w Thierbach w NRD" Przegląd Geodezyjny, 1969

[20] J. Ågren, R. Svensson, „Postglacial Land Uplift Model and System Definition for the New Swedish Height System RH 2000", 2007